Working Paper 84-5

The Use of A Flat-Plate Current Meter In Nearshore Flows

D. K. Hollingsworth, F. Y. Sorrell and T. B. Curtin

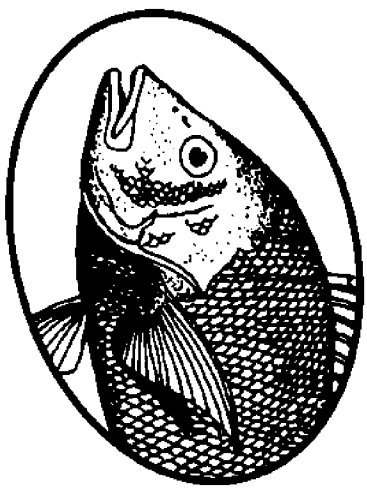

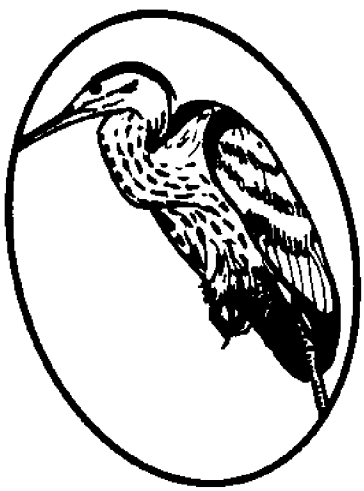

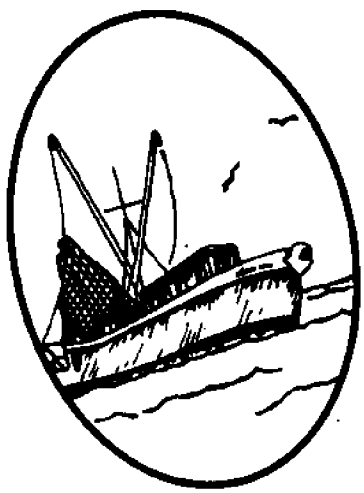

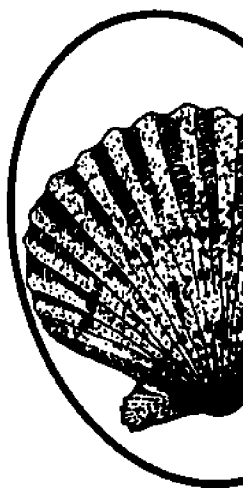

UNC Sea Grant College Program
105 1911 Building
North Carolina State University
Raleigh, NC 27650

THE USE OF A FLAT-PLATE CURRENT METER IN NEARSHORE FLOWS

by

D. K. Hollingsworth(1)

F. Y. Sorrell(1)

T. B. Curtin(2)

(1) Department of Mechanical and Aerospace Engineering
(2) Department of Marine, Earth and Atmospheric Sciences
North Carolina State University
Raleigh, North Carolina 27695-7910

This work was sponsored by the Office of Sea Grant, NOAA, U.S. Department of Commerce, under Grant No. NA81AA-D-00026 and the North Carolina Department of Administration. The U.S. Government is authorized to produce and distribute reprints for governmental purposes notwithstanding any copyright that may appear hereon.

UNC Sea Grant College Publication UNC-SG-WP-84-5

May, 1984

$2.25

ABSTRACT

An experimental investigation was conducted of the forces arising from an unsteady flow against a flat plate used as the drag body in a drag-force current meter. A current meter was constructed for the purpose of measuring flow in the nearshore region of the ocean. An experiment was conducted to characterize the response of the sensor to an unsteady flow. The current meter was subjected to both an oscillatory and mean flow simultaneously. This was accomplished by sinusoidally oscillating the sensor while translating it down a water channel. Fourier analysis of the data yielded instantaneous and cycle-averaged values of the drag and mass coefficients for the plate.

The cycle-averaged values of the coefficients were correlated with a nondimensional parameter which is proportional to the ratio of the steady component of the drag force to the unsteady component. This correlation indicates that for large values of this parameter, the cycle-averaged value of the drag coefficient becomes constant and equal to the value found for steady flow. The variation of the instantaneous values of the coefficients through the velocity oscillation were examined and an attempt was made to correlate the behavior of the coefficients with the coefficients of the non-dimensional parameter. The ability of the current meter to accurately measure the mean value of the sinusoidal flow oscillations was correlated to the nondimensional parameter and was shown to improve for large values of the parameter.

TABLE OF CONTENTS

LIST OF TABLES

LIST OF FIGURES

LIST OF SYMBOLS

A = cross-sectional area of drag body

A_F = force calibration constant

A_T = tare force calibration constant

A_n = coefficient of n^{th} sine term in Fourier expansion

B_n = coefficient of n^{th} cosine therm in Fourier expansion

C_d = constant drag coefficient in Morison's equation

$\overline{C_d}$ = cycle average drag coefficient

$C_d(\vartheta)$ = instantaneous drag coefficient

C_{ds} = steady flow drag coefficient

C_m = constant mass coefficient in Morison's equation

$\overline{C_m}$ = cycle average mass coefficient

$C_m(\vartheta)$ = instantaneous mass coefficient

D = length scale of drag body

D_n = coefficient of n^{th} term in sine θ |sine θ| expansion

$\frac{du}{dt}$ = free stream fluid acceleration

F = total force measured by sensor

F^* = hydrodynamic force coefficient (EQ 5.8)

F_{FD} = maximum profile drag force

F_H = hydrodynamic force

F_I = maximum inertial force

$\overline{F_{SQ}}$ = cycle average of the square root of the force coefficient

F_{TARE} = tare force measured by sensor

I = counter for discrete data points in the representative waveform

K = Keulegan-Carpenter period parameter (EQ 1.2)

K^* = extended period parameter (EQ 5.11)

n = counter for individual terms in a Fourier series

N = number of discrete values in the representative waveform

R_o = nondimensional mean velocity coefficient (EQ 5.11)

R_1 = nondimensional oscillatory velocity coefficient (EQ 5.11)

R_c = maximum oscillator displacement

$R(\theta)$ = nondimensional velocity coefficient

t = time

T = period of velocity oscillation

U = free stream velocity

U_o = average velocity

U_1 = maximum oscillatory velocity

U^* = velocity calculated from sensor output using the steady flow model (EG 5.31)

V = sensor output

$\forall$ = volume of fluid surrounding the drag body

V_o = sensor output in the absence of flow

x = instantaneous oscillator displacement

ρ = fluid density

θ = phase angle

θ_1 = phase angle for negative-going zero crossing for $U_o < U_1$ case

θ_2 = phase angle for positive-going zero crossing for $U_o < U_1$ case

1. INTRODUCTION

The nearshore region of the ocean is the primary interface between man and the marine environment. The nearshore, along with the surface and the bottom, is one of the three boundary layer regions of the ocean. The nearshore boundary layer is defined here as extending from the breaker zone out to a depth of approximately 60 meters. Nearshore transport processes link the estuarine and marine environments. The measurement of water velocity and temperature in the nearshore boundary layer can provide information useful in the proper management of man's interaction with these environments.

A suitable measurement system is obviously a requirement to analyze the physical dynamics of ocean boundary layer regions. The nearshore flow field may be composed of several types of motion, including large- and small-scale turbulence, wind waves, long waves, convection, advection and tidal flow. Therefore, the system must accurately measure an unsteady component of motion superimposed on a mean velocity. Langrangian systems measure specific particle paths typically by the use of drogues or dye traces. This technique is useful in the evaluation of pollutant (e.g., oil spills) or mass transport models. However, this method is deficient in providing quantitative results that lend themselves to statistical analysis of the field of motion. Fixed-point or Eulerian systems involve the use of an array of moored current meters. The data can be used to generate a quantitative analysis of the mass and momentum fluxes through the array.

There are several commercially available current meters that can be used in fixed-point mooring systems. The average cost per unit ($5,000 to $15,000) limits the use of these instruments in sufficient quantities to achieve the high resolution necessary in three-dimensional, boundary-layer studies. In addition, the velocity transducers in most of these units have limited, high frequency response and/or threshold speed.

To reduce the cost of a nearshore experiment to a feasible amount, a mooring system was designed which uses one multi-channel data recorder interfaced to several velocity and temperature sensors distributed over the water column. A number of velocity sensors were considered with regard to cost, frequency response, threshold speed, long-term calibration stability, resistance to biofouling, and ability to accurately resolve orthogonal components of motion. These sensor designs fall into three classes: thermal boundary layer, electromagnet and mechanical. The thermal, boundary-layer sensors (e.g., hot film, hot wire, thermistor chain) measure the voltage necessary to maintain an electrical resistance element of a constant temperature as the heat transfer from the element varies with flow velocity. These instruments are extremely susceptible to biofouling and the calibration of the sensor varies with water temperature. Electromagnetic sensors measure the small voltage induced as the sodium and chloride ions in seawater move through a magnetic field produced by the sensor. The microvolt level signal must be detected in a millivolt noise level environment. One component of this noise arises from the instability of the potential of the electrodes used to detect the signal. This drift in the electrode potential causes an instability in the calibration curve. The quality of the electronics necessary to resolve the signal under these conditions causes these instruments to be more expensive than other designs. Mechanical sensor

designs usually involve counting the turns of a rotor or propeller. These instruments have bearing surfaces which are susceptible to biofouling and corrosion. The hydrodynamics of lthe propeller or rotor varies with degree of biofouling. These sensors often have poor frequency response due to the inertia of their rotating parts.

One sensor design which satisfied many of the requirements was that of the drag-force current meter. This instrument consists of a bluff body attached to a force-measuring transducer. In the present work a flat plate is used as the bluff body. The body is exposed to the flow and the hydrodynamic drag force on the body is measured and recorded. Given an adequate understanding of the relationship between velocity and the resultant drag force, these force recordings can be reduced to yield a measurement of the flow velocity at that point. Such an instrument was expected to be relatively inexpensive to construct. The calibration of the transducer can be compensated for temperature variations. Unlike other mechanical designs, this sensor has no rotating parts or bearing surfaces; therefore, the calibration curve should be less sensitive to biofouling and corrosion. Coating the bluff body with anti-fouling paint further minimizes the effect of biofouling on the performance. The use of two separate drag bodies at right angles, or one symmetric body, allows orthogonal force components to be resolved and recorded.

The relationship between hydrodynamic force and velocity is well understood for steady flow in the range of Reynolds numbers (10^3 to 10^6 for the instrument used in this work) that normally occurs in the nearshore environment. However, this relationship is not well understood for an unsteady flow, particularly in the presence of a mean-velocity component. The usefulness of the drag-force current meter is obviously limited without a full understanding of the forces generated in such an unsteady flow.

Potential flow theory indicates that the force on an object in an unsteady flow is proportional to the acceleration of the free stream fluid. In 1950, O'Brien and Morison [1] combined this effect with the standard, turbulent-profile drag expression to form Morison's equation:

$$F_H = 1/2\ C_d \rho A\ U|U| + C_m\ \rho\ \Psi \frac{dU}{dt} \qquad (1.1)$$

where

F_H = total force on the object (dynes)

C_d = drag coefficient

C_m = mass coefficient

ρ = density (gm/cm^3)

A = cross-sectional area of the object exposed to the Flow (cm^2)

Ψ = volume of fluid associated with the object (cm^3)

U = free stream fluid velocity (cm/sec)

$\frac{dU}{dt}$ = free stream fluid acceleration (cm/sec^2)

The first term in the equation is the steady flow profile drag. The second term is propertional to the force required to accelerate the mass of fluid displaced by the object. Morison's equation is one of the more generally accepted models of hydrodynamic force on an object exposed to an accelerating viscous fluid flow.

Inman and Nasu [2] constructed what is perhaps the first drag-force current meter used to measure nearshore flows. A sphere was used as the bluff body in this instrument. The effect of fluid acceleration was investigated by oscillating the sensor in air and water. Such tests showed that the acceleration term in Morison's equation could not be neglected relative to the profile drag term. Furthermore, the mass coefficient was found to be a function of the period of oscillation. Because oof these characteristics, the sensor was used to record only crest and trough values of the orbital wave velocity. Such values were thought to occur at times when the free stream acceleration is zero, and the force is a function of velocity only.

Beardsley, et al. [3] built and tested a sensor that used a fine wire mesh formed into a cylinder as the drag body. The sensor was tested by oscillating it in still water. These tests indicated that because oof the cylinder's small size (0.318 cm I.D.), there was no appreciable effect of fluid acceleration on the total hydrodynamic force. A wire mesh was used in preference to a solid cylinder because it was thought that a mesh cylinder is less likely to be affected by vortex shedding. Such vortex shedding causes an oscillating force perpendicular to the flow direction. This force is indistinguishable from free stream turbulence at the shedding frequency and would result in contamination of the sensor output.

Smith and Harrison [4] addressed the problem of vortex shedding by using a perforated sphere as a drag body. Tests in steady flow showed that such perforations attenuated the forces arising from the vortices, but no tests were reported concerning the performance of the sensor in unsteady flow. They required that the sensor be used in a flow where the kunsteady component is small enough that the profile drag term alone is sufficient to calculate the velocity. However, Smith and Harrison so not precisely define the values of lmean and oscillatory velocity or the period of oscillation that constitutes sufficiently a small unsteady component.

Experimental data useful in analyzing kthe response of a drag-force current meter in an unsteady flow have been reported by Keulegan and Carpenter [6]. They experimenttally determined the instantaneous and cycle-average values of C_m and C_d for plates and cylinders in a fluid (water) that was undergoing sinusoidal oscillations. The flow oscillations had a zero mean, and only two-dimensional bodies were considered. Their results showed that the coefficients varied throughout the period of the oscillation. That is, the values of C_d and C_m were not constant in time. The values of C_d and C_m averaged over a complete cycle were shown to vary as a kfunction of the period parameter:

$$K = \frac{U_1 T}{D} \tag{1.2}$$

where

U_1 = amplitude of the velocity oscillation (cm/sec)

T = period of the oscillation (sec)

D = diameter of the cylinder or width of the plate (cm^2)

K is often referred to as the Keulegan-Carpenter parameter and is proportional to the rtio of the distance travelled by a fluid particle during half of a velocity cycle to the size of the bluff body.

The question of error resulting from using a drag-force sensor to measure flow velocity using only the steady flow term in Equation (1.1) was addressed by Olson [7]. In his analysis, he used the average values of C_d and C_m from the work of Keulegan and Carpenter. Olson considered a sensor based on a cylindrical drag body. His calculations showed that if Keulegan and Carpenter's results were valid for non-zero mean flow, serious errors in instantaneous and average velocity would result from neglecting the acceleration effect. These results were based on cycle averaged values of C_d and C_m, and a mean flow that was smaller than the oscillatory component. Olson also showed that reducing the diameter of the cylinder would reduce the effect of acceleration relative to the profile drag. However, a considerable reduction in frontal area would reduce the total force on the body to a value that would be difficult to measure.

These investigations lead to the following general conclusions:

1. In a nearshore flow, both the velocity and the acceleration are unknown. Moreover, the mass coefficient may vary with frequency, which is also unknown. Therefore, the instrument should be used in a flow in which the first term in Equation (1.1) is sufficient to calculate the velocity from the measured force.

2. There exists a poor understanding of what combinations of mean velocity and acceleration constitute such a flow regime.

3. A significant reduction in the size of the drag body reduces the effect of free stream acceleration. However, such a reduction impairs the ability of the sensor to measure small velocities.

4. Because forces arising from vortex shedding are a consideration, especially when bluff drag bodies are used, an effort should be made to keep vortex shedding (and the accompanying sensor response) to a minimum or at least predictable.

2. OBJECTIVES

The purpose of this work was to investigate the forces arising from an unsteady flow against a flat plate used as the drag body in a drag force current meter. The reasons for choosing a plate as the drag body are given in Section 3. The experiment consisted of subjecting the sensor to both an oscillatory and mean flow simultaneously. This was accomplished by sinusoidally oscillating the current meter while translating it down a towing tank. The amplitude and period of the oscillations were varied as well as the translation velocity. The drag and mass coefficients thus obtained were examined with respect to the following considerations:

1. the behavior of the instantaneous and average values of the coefficients in the presence of a non-zero mean flow as compared to a zero mean flow;

2. the ability to correlate the variations in the average values of C_d and C_m with a non-dimensional prameter that includes the effect of a non-zero mean velocity;

3. the usefulness of such a correlation in determining values of velocity and acceleration that give an acceptable sensor performance.

3. DESCRIPTION OF THE FLAT PLATE CURRENT SENSOR

3.1. Use of a Flat Plate as the Drag Body

A plate was chosen as the drag body of the current meter for several reasons:

1. The published, steady-flow drag coefficient [8] for a square, flat plate (C_d = 1.17) is approximately that of a circular cylinder (C_d = 1.18 for two-dimensional flow), and higher than that of a sphere (C_d = 0.47). A large drag co-efficient increases the sensitivity of the instrument for a given cross-sectional area of the drag body.

2. The point on a symmetric body from which vorticies originate may shift as the flow conditions change or as biofouling occurs. On a flat plate, this point is stabilized at the edges. Such stability may lessen the effect of vortex shedding or make the effect more predictable. The corners of the plate were rounded in an attempt to avoid an interaction between vorticies shed from two adjoining edges.

3. The possibility of using a flat plate in a sensor of this type has not been previously evaluated. Drag and mass coefficients have been determined for a two-dimensional plate in a sinusoidally oscillated flow with zero mean [7]. However, no such experiments were known in which the coefficients were determined for an oscillatory component superimposed on a mean flow. This case is not only of importance in current-meter design, but it is also a rather poorly understood area of the general subject of forces on bodies in unsteady flows.

3.2. General Description of the Instrument

Two, flat-plate and force-transducer assemblies were used to measure the horizontal, hydrodynamic force vector. Each transducer was composed of a cantilevered beam with two strain gages attached to the beam near the cantilever point. The plate (A = 161.3 cm^2) was attached to the free end of the beam. The maximum strain experienced by each beam could be set by an adjustable stop. A description of the physical characteristics of the transducer assemblies and associated electronics is given in Appendix 8.1. The cantilevered beams were attached to an aluminum frame that formed the protective cage for the drag bodies (Figure 3.1). One end of the frame was fastened to a length of PVC pipe that served as the electronics case. Wires from the transducers passed through the end of the case adjoining the frame. A cable connecting the sensor to a power supply and data recorder passed through an O-ring sealed plug on the other end of the case. The sensor housing could be attached in mechanical series with the spar of a fixed-point mooring system. The frame would be a stressed member in such a system.

In steady flow, the force seen by the transducer plates is described by the first term in Equation (1.1). The velocity is thus determined by:

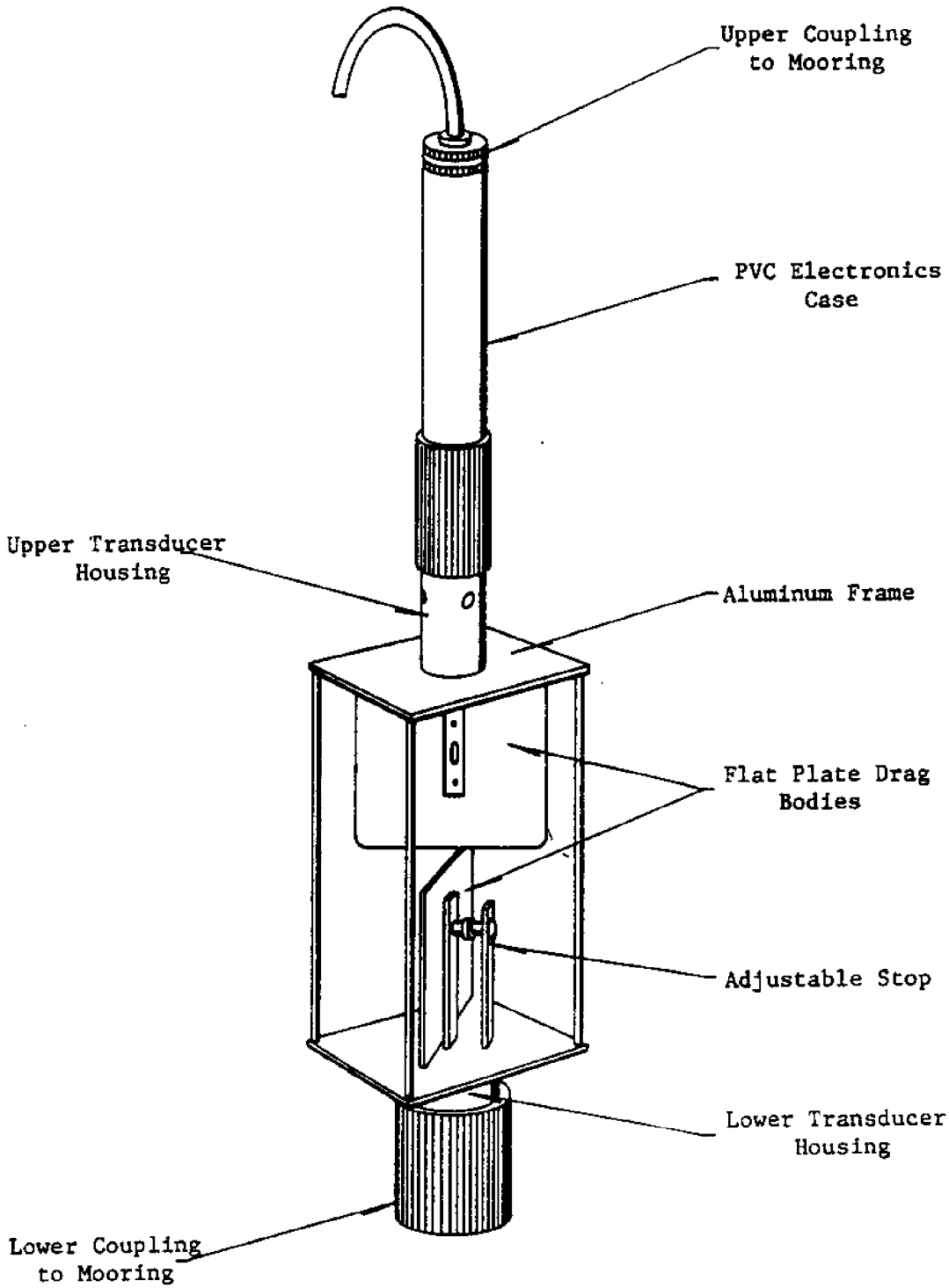

Figure 3.1. Flat Plate Current Meter

$$U = \left| \frac{2F_H}{D_{ds}\ \rho A} \right|^{1/2} \qquad (3.1)$$

where

C_{ds} = steady-flow drag coefficient

F_H = hydrodynamic force measured by the transducers

This relationship was verified as part of the unsteady flow experiment. The threshold velocity of the sensor in steady flow is approximately 5 cm/sec. This velocity corresponds to a strain at the gage site of approximately 6 ucm/cm, which is the practical lower limit of the transducer assemble. The need for long-term zero stability limited the maximum value of the strain to about 1500 ucm/cm. For the 12.7 cm by 12.7 cm plate used, this strain corresponds to an upper velocity limit of 80 cm/sec. In higher velocity flows, a smaller plate can be used to raise the upper velocity limit at the expense of a loss of threshold sensitivity.

4. DESCRIPTION OF THE EXPERIMENT

4.1. Force Calibration of Current Meter

A voltage output versus force input calibration was performed for each flat-plate transducer. This force to voltage relationship was obtained by placing the sensor such that one of the plates was in a horizontal position. The output voltage was recorded as weights varying in mass from 1 gm to 400 gm were placed on a bracket attached to the center of the plate. The calibration for the upper transducer used in the unsteady flow experiment is given in Figure 4.1. The calibration constant obtained for this transducer was 1.108×10^{-5} volts/dyne.

4.2. Determination of the Tare Voltage

When the mass of the plate and cantilevered beam is accelerated, a force (and thus an output voltage) is produced which is proportioned to the acceleration. Past investigators have termed this voltage the "tare voltage." In the unsteady flow experiment, the current meter was accelerated by the sinusoidal oscillatyor described in Section 4.3.3. The raw output of the sensor was composed of a voltage proportional to the hydrodynamic force, and the tare voltage proportional to the acceleration of the sensor. The tare voltage was determined as a function of acceleration and subtracted from the raw output as part of the data reduction for the unsteady flow experiment. To determine the tare voltage for the upper transducer, the current meter was oscillated in air with the sinusoidal oscillator. By accelerating the transducer at low speeds in air, the hydrodynamic forces are negligible and the output is representative only of the tare force.

The tests in air showed the tare voltage to be proportional to, and in phase with, the sinusoidal acceleration produced by the oscillator. A plot of tare voltage versus peak acceleration for the upper transducer is given in Figure 4.2. The tare voltage calibration constant was found to be 4.0×10^{-3} volts/cm/(sec^2).

4.3. Unsteady Flow Experiment

4.3.1. General Description

The hydrodynamic force data were obtained by subjecting the flat-plate current sensor to a range of oscillatory flow velocities, frequencies and mean velocities that were representative of the nearshore environment. The sensor was sinusoidally oscillated by a mechanism attached to a carriage mounted on rails above a towing tank. Translating the carriage down the length of the tank imparted a mean velocity to the sensor. The output from the upper transducer of the sensor, along with a trace of the motion of the oscillator was recorded on an FM cassette deck for later computer analysis. These output traces were also recorded on a dual-channel stripchart recorder.

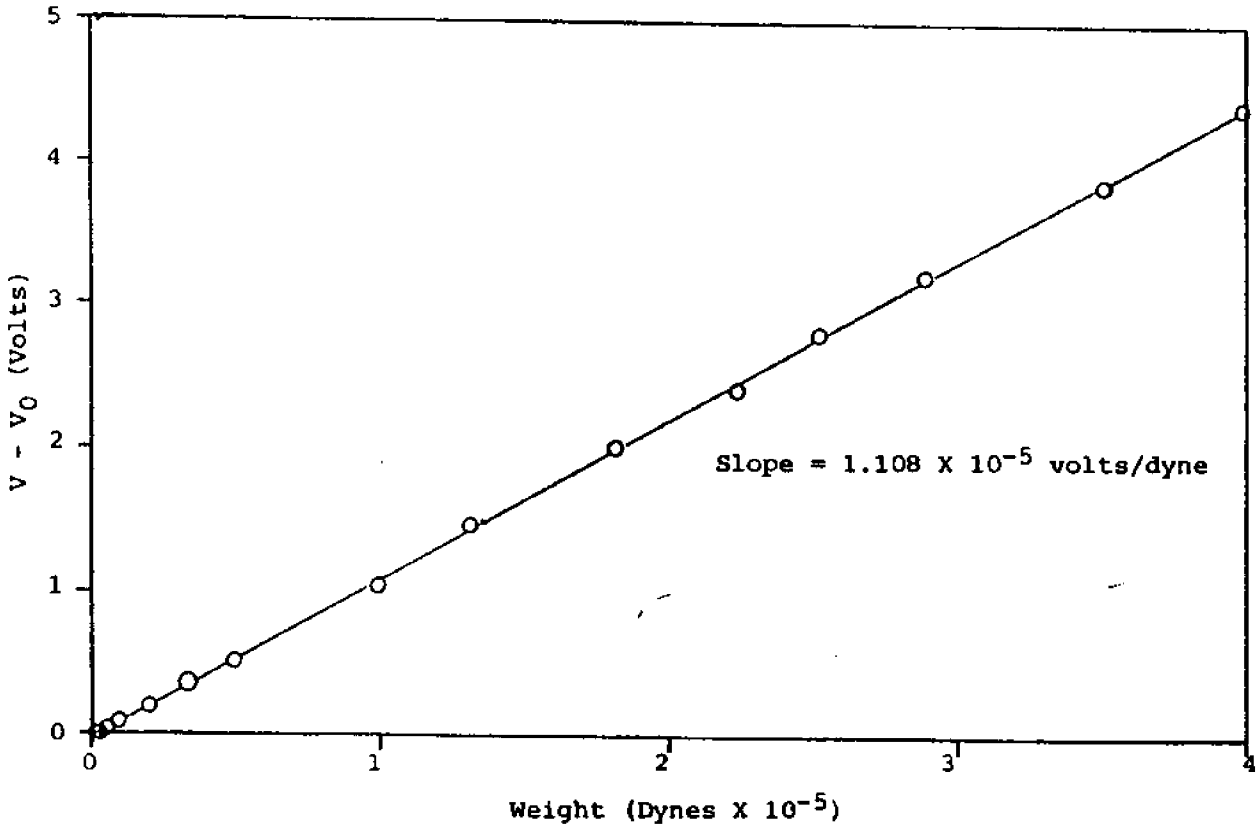

Figure 4.1. Dead Load Calibration of Current Meter

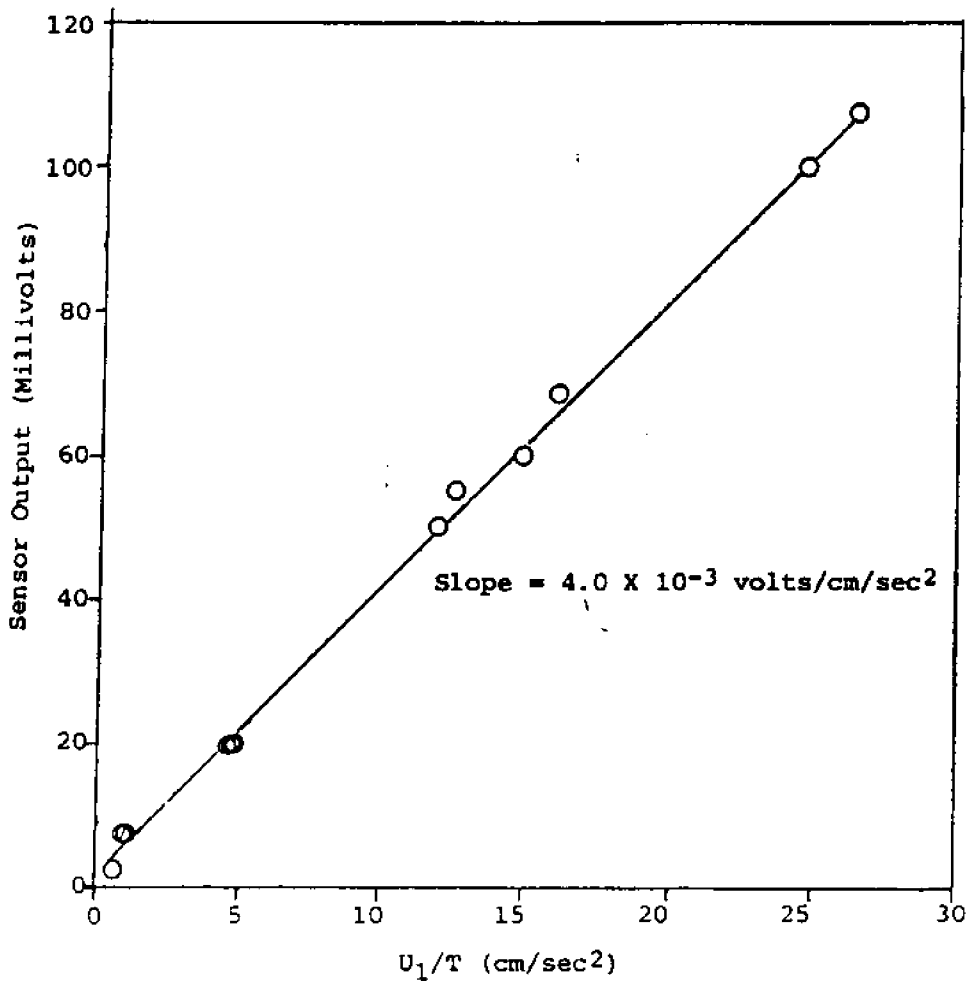

Figure 4.2. Tare Voltage Versus Peak Acceleration

4.3.2. Towing Tank

The towing tank used for these tests was located at the Environmental Protection Agency Fluid Modeling Facility in Research Triangle Park, North Carolina. The tank was 25 m long and 2.5 m wide and was filled to a depth of approximately 1 m with a saline solution which had a density of 1.135 gm/cc. Blocking effects associated with smaller tanks were minimized by using such a large tank.

The oscillator, power supply and data recorders were placed on a large carriage which ran on rails above the tank. The sensor was suspended from the oscillator such that the upper velocity sensor was at approximately mid-depth in the tank. A continuous cable system pulled the carriage through a 10 m long test section. The cable was driven by an electromagnetic clutch with controlled slippage which was in turn driven by a constant speed D. C. motor. The system is capable of moving the carriage at speeds of 0 to 49 cm/sec. The ends of the test section were defined by microswitches which turned a digital timer on as the carriage entered the section and off as it completed the 10 m run. The average velocity of the carriage was calculated by dividing the length of the section by the time required for the carriage to traverse that length. Ample space was available to accelerate the cart to a constant speed before it entered the test section.

4.3.3. Oscillator

A mechanical oscillator was used to impart a sinusoidal velocity to the current meter. The type of oscillator used in this experiment was a Scotch yoke mechanism [9]. The mechanism was driven by a variable speed D. C. motor capable of driving the oscillator at frequencies from 0.1 Hz to 1 Hz. The oscillator incorporated a variable length crank capable of producing displacement amplitudes of 15.9, 12.7, 10.2, 7.6, 5.1, and 2.5 cm. Various combinations of crank length and motor speed yielded a range of amplitudes and periods of oscillation. The motion produced by the oscillator was measured with a displacement transducer, and the output was recorded along with the sensor output.

4.3.4. Procedure

The tests were performed by setting the amplitude and frequency of the oscillator to yield a desired oscillatory velocity and then running the cart through the test section at mean velocities of approximately 10,20, and 40 cm/sec. After these three runs the oscillator setting would be changed and the runs would be repeated. Before the tests were begun, the FM cassette deck was calibrated to known voltages. A repeat of this calibration at the end of the tests showed that no appreciable change in calibration had occurred. The raw data from this experiment consisted of the density of the salt water, the length of the test section, the calibration constants of the cassette deck, the amplitude setting and run duration for each run, and the recordings of oscillator displacement and sensor output.

Included in these tests was a set of four runs in which the oscillator was not running. This set of runs defined the steady flow drag coefficient for the sensor over the range of mean velocities of interest.

5. DATA REDUCTION

5.1. General Description

The data reduction involved calclulating the time average and instantaneous values of C_d and C_m given the raw data from the unsteady flow experiment. The coefficients obtained from the runs with a zero mean velocity were compared with those obtained by Keulegan and Carpenter for a two-dimensional plate in a zero mean flow. The average values of the coefficients were then plotted against a non-dimensional parameter in an attempt to extend the correlation with the period parameter to flows with a non-zero mean component. This parameter is termed the extended period parameter and can be shown to be proportional to the maximum force occurring in the cycle due to steady-flow profile drag divided by the maximum force due to the inertial term in Equation (1.1). Finally, this parameter was used to quantify the ability of the instrument to measure the average velocity in a sinusoidal unsteady flow.

5.2 Steady Flow Drag Coefficient

The steady-flow drag coefficient, C_{ds}, was determined from recordings of four runs in which the oscillator was not running. C_{ds} was calculated using the first term in Equation (1.1):

$$C_{ds} = \frac{2V}{A_F \rho D^2 U^2} \tag{5.1}$$

where

A_F = force calibration constant (1.108×10^{-5} volts/dyne)

V = sensor output (volts)

D^2 area of the square flat plate (cm^2)

Table 5.1 contains the values of C_{ds} for each run. The average of these values is 1.25. This value is hereafter used as the value of C_{ds}.

Tabel 5.1. Values of Steady Flow Drag Coefficient

U_o (cm/sec)	C_{ds}
10.192	1.23
19.876	1.25
40.019	1.23
44.090	1.27

5.3. Preparation of Representative Data Set

The tape recordings of the oscillator position and sensor output trace were digitized and entered into the memory of a Data General Eclipse computer. The two signals were filtered and sampled simultaneously using identical filters; therefore, no phase shift between the signals occurred due to sampling technique. Tests of the filters confirmed the absence of a phase shift. The cutoff frequency of the low pass filters was 3 Hz, and the highest oscillatory frequency was less than 1 Hz. After filtering, the signals were sampled at 0.02 sec intervals by a 10-bit analogue-to-digital converter. The recordings for each run were sampled 2,048 times for a total digitized record length of 40.96 sec. Since the velocity input to the current meter was cyclic, the output voltage from the sensor was also cyclic in nature. An average, sensor-output cycle for each run was prepared from the digitized records by averaging a number of the sensor-output cycles from a given record. The number of cycles used to generate the average varied from 6 for high-frequency oscillations to 2 for low-frequency oscillations with a high mean velocity. Examples of the latter case were runs with oscillator periods of 9 to 10 sec and carriage run times of 22 to 24 sec. For these cases only two complete oscillations occured within the length of the test section. The starting point for each of these oscillations was determined by examining the digitized record of the oscillator motion. The peaks of this sinusoidal trace were defined to be the endpoints of the velocity input cycle. The endpoints of the sensor-output cycles were taken to be coincident with those of the input cycle with the oscillator motion defined as:

$$x(t/T) = - R_c \cos(2\pi t/T) \tag{5.2}$$

The velocity input to the current meter is:

$$U(t/T) = U_o + U_t \sin(2A\pi t/T) \tag{5.3}$$

TABLE 5.2. Velocity Input Data

Run No.	U_o/U_1	U_o (cm/sec)	U_1 (cm/sec)	T* (sec)
1	0.00	0.00	23.36	4.90
2	0.00	0.00	24.18	3.30
3	0.00	0.00	18.00	2.66
4	0.00	0.00	21.71	2.94
5	0.00	0.00	15.80	2.02
6	0.00	0.00	9.97	1.60
7	0.95	10.17	10.68	9.34
8	1.86	19.85	10.66	9.36
9	4.14	44.18	10.68	9.34
10	1.35	10.18	7.53	8.48
11	6.52	19.90	3.05	10.46
12	5.84	44.12	7.56	8.48
13	0.44	10.19	23.30	2.74
14	0.84	19.89	23.64	2.70
15	2.28	45.13	19.83	3.22
16	5.86	10.66	1.82	8.76
17	10.55	19.84	1.88	8.50
18	1.89	10.20	5.39	2.96
19	3.68	19.85	5.39	2.96
20	8.19	44.16	5.39	2.96
21	2.87	10.20	3.56	8.96
22	5.60	19.87	3.55	8.98
23	12.30	44.14	3.59	8.88
24	0.36	10.12	28.50	1.12
25	0.70	19.84	28.50	1.12
26	1.36	40.24	29.55	1.08

*Estimated Maximum Error in T is ±.08 sec. U_1 calculated from $U_1 = 2\pi L/T$ where L = Oscillator arm length.

$$U_1 = \frac{2\pi R_c}{T} \tag{5.4}$$

where

R_c = oscillator crank length (cm)

t = time into the waveform (sec)

T = period of the oscillation (sec)

U_1 = peak oscillatory velocity (cm/sec)

U_o = mean velocity (cm/sec)

The period of an individual velocity cycle was determined by counting the number of points from one peak in the motion trace to the next. The period of the average output cycle was equal to the average of the periods of the output cycles used to construct it. This average was typically within 2 points (0.04 sec) of the period of any given constituent cycle. The mean velocity, U_o, was determined by dividing the length of the test section (10 m) by the duration of the run. Table 5.2 contains the values of U_o, U_1, and T for each run.

The average output force for each run is proportional to the time varying force on the flat-plate drag body caused by the velocity input described by Equation (5.3). This force is a sum of the hydrodynamic forces and the "tare force":

$$F(t/T) = F_H(t/T) + F_{TARE(t/T)} \tag{5.5}$$

$$= \frac{[V(t/T) - V_o]}{A_F} \tag{5.6}$$

where

V_o = output of sensor in the absence of any flow (volts)

The tare force was found to be proportional to the acceleration of the sensor and can be expressed in terms of U_1 and T:

$$F_{TARE}(t/T) = \left|\frac{A_T}{A_F}\right| \left|\frac{U_1}{T}\right| \cos \left|\frac{2\pi t}{T}\right| \tag{5.7}$$

where

A_T = tare voltage calibration constant (4.0×10^{-3} volts $(sec^2)/cm$)

The nondimensional hydrodynamic force coefficient used in this analysis was defined as:

$$F^*(t/T) = \frac{F_H(t/T)}{\rho D^2 (U_o + U_1)^2}$$

$$= \frac{F(t/T)}{\rho D^2 (U_o + U_1)^2} - \frac{F_{TARE}(t/T)}{\rho D^2 (U_o + U_1)^2} \qquad (5.8)$$

Equation (5.5) is therefore nondimensionalized by a value proportional to the maximum steady flow drag force that occurs in the cycle. The average voltage output cycle for each run was converted into a time series of this nondimensional force coefficient through the application of Equations (5.6), (5.7), and (5.8). The time series thus formed is hereafter referred to as the "representative waveform" for each run. Equation (1.1) can be similarly nondimensionalized to yield:

$$F_H = \frac{C_d U|U|}{2(U_o + U_1)^2} + \frac{C_M \forall}{D^2(U_o + U_1)^2} \frac{dU}{dt} \qquad (5.9)$$

The fluid volume, $\forall$, was defined as a cylindrical volume enclosing the flat plate (7):

$$\forall = \frac{\pi D^3}{4}$$

Given the sinusoidal velocity input, the force on the flat plate was modeled as:

$$F^*(\theta) = \frac{C_d}{2}(R_o + R_1 \sin(\theta))\left|R_o + R_1 \sin(\theta)\right| + \frac{C_m \pi^2}{2K^*}\cos(\theta) \qquad (5.10)$$

where,

$$\theta = \frac{2\pi t}{T} \quad R_o = \frac{U_o}{(U_o + U_1)} \quad R_1 = \frac{U_1}{(U_o + U_1)} \quad K^* = \frac{K}{R_1^2} = \frac{U_1 T}{D}\left|\frac{U_o}{U_1} + 1\right|^2 \qquad (5.11)$$

Equation (5.10) is the model used to determine the values of C_d and C_m for each representative waveform.

Equation (5.11) defines the extended period parameter, K*, as a nondimensional grouping made up of the Keulegan-Carpenter period parameter, K, and a term containing the ratio of mean velocity to peak oscillatory velocity. K* is therefore seen as a parameter which may extend the correlation of C_d and C_m with K in zero mean flow to oscillatory flows with a non-zero mean component. Chapter 6 contains plots of the cycle average values of C_d and C_m versus K* for both zero and non-zero mean flows. Note that in the absence of ean flow, K* reduces to the period parameter K.

5.4. Determination of the Coefficients

Fourier series analysis was employed by Keulegan and Carpenter to determine both the average and instantaneous values of the coefficients for zero mean flow. This technique was expanded in the present work to include the effect of a non-zero mean velocity. In this analysis, the representative wave form for each run was assumed to be represented by an infinite sum of sine and cosine terms:

$$F^*(\theta) = \frac{A_o}{2} + A_1 \sin(\theta) + A_2 \sin(2\theta) + A_3 \sin(3\theta) + \cdots + B_1 \cos(\theta) + B_2 \cos(2\theta) + B_3 \cos(3\theta) + \cdots + \qquad (5.12)$$

where the Fourier coefficients are defined by:

$$A_o = \frac{1}{\pi}\int_o^{2\pi} F^*(\theta)\, d\theta \qquad (5.13)$$

$$A_n = \frac{1}{\pi} \int_0^{2\pi} F^*(\theta) \sin(n\theta)\, d\theta \qquad n > 1 \tag{5.14}$$

$$B_n = \frac{1}{\pi} \int_0^{2\pi} F^*(\theta) \cos(n\theta)\, d\theta \qquad n > 1 \tag{5.15}$$

These integrals are approximated by finite summations for use with the discrete values of the representative waveforms by:

$$A_o = \frac{2}{N} \sum_{I=1}^{N} F^*(I) \tag{5.16}$$

$$A_n = \frac{2}{N} \sum_{I=1}^{N} F^*(I) \sin(n\theta) \qquad n > 1 \tag{5.17}$$

$$B_n = \frac{2}{N} \sum_{I=1}^{N} F^*(I) \cos(n\theta) \qquad n > 1 \tag{5.18}$$

where:

N = number of discrete values in the representative waveform record

$$\theta = \frac{2\pi(I-1)}{N}$$

Thus, A_n and B_n could be computed for each run. C_d and C_m were then computed from the values of A_n and B_n. The details of the method used to obtain the coefficients depend on the values of U_o and U_1. The runs were therefore divided into three cases: $U_o = 0$, $U_o > U_1$, and $U_1 < U_o$. A computer program based on this model was written for each case. These programs produced the numerical values of C_d and C_m. Appendix 8.2 contains a derivation of the method for the three cases. The results of the derivation for each case are presented here. Table 5.3 contains the average values of the drag and mass coefficients along with the value of K* for each run.

Table 5.3. Average Values of C_d and C_m

Run No.	K*	C_d	C_m
1	7.854	2.914	1.794
2	6.283	3.158	1.896
3	4.770	4.086	1.704
4	5.026	3.648	1.871
5	2.513	5.616	1.521
6	1.257	7.182	1.136
7	29.939	1.293	0.856
8	64.360	1.200	1.454
9	207.287	1.185	1.252
10	27.820	1.168	1.287
11	142.179	1.347	3.431
12	234.629	1.155	2.256
13	10.384	0.789	1.876
14	17.039	0.884	1.648
15	53.951	1.288	1.466
16	58.994	1.526	1.727
17	168.106	1.314	2.259
18	10.512	0.766	1.087
19	27.545	1.280	1.273
20	106.151	1.272	2.271
21	37.523	1.312	1.529
22	109.145	1.396	1.928
23	443.331	1.288	2.260
24	4.615	1.941	0.942
25	7.228	1.490	0.815
26	14.013	1.030	0.595

$U_o = 0$ Case

For the zero mean flow case, the representative waveform is symmetric in time:

$$F^*(\theta) = -F^*(\theta + \pi) \tag{5.19}$$

Thus, the even Fourier coefficients are taken to be zero. For this case, the expressions for the average values of the drag and mass coefficients are:

$$\overline{C_d} = \frac{2A_1}{D_1} \tag{5.20}$$

$$\overline{C_m} = \frac{2K^*B_1}{\pi^2} \tag{5.21}$$

The instantaneous values of C_d and C_m were given by:

$$C_d(\theta) = \overline{C_d} + 2 \sum_{n=1}^{Z} \frac{[A_{2n+1} - D_{2n+1}\,\overline{C_d}/2]}{\sin(\theta)\,|\sin(\theta)|} \sin[(2n+1)\theta] \tag{5.22}$$

$$C_m(\theta) = \overline{C_m} + 2K^* \sum_{n=1}^{Z} B_{2n+1} \frac{\cos[(2n+1)\theta]}{\pi^2 \cos\theta} \tag{5.23}$$

where

$$D_n = \frac{1}{\pi} \int_0^{2\pi} |\sin(\theta)| \sin(\theta) \sin(n\theta)\, d\theta$$

Z = number of terms taken in the finite series

In the computer program used to calculate the values of the coefficients, Z was equal to 3 for C_d and 4 for C_m. The derivation of these results is contained in Appendix 8.2.

$U_o > U_1$ Case

For the runs in which the mean velocity is greater than the maximum oscillatory components, the representative waveform was asymmetric. This asymmetry is due to the square law dependency of the profile drag term. For this case, the average values of the drag and mass coefficients were given by:

$$\overline{C_d} = \frac{A_o}{(R_o^2 + R_1^2/2)} \tag{5.24}$$

$$\overline{C_m} = \frac{2K^*B_1}{\pi^2} \tag{5.25}$$

The expressions for the instantaneous values of the coefficients are:

$$C_d(\theta) = \overline{C}_d + \frac{2}{(R_o + R_1 \sin\theta)^2}\left[\sum_{n=1}^{\infty} A_{2n+1} \sin[(2n+1)\theta] + \sum_{m+2}^{\infty} B_{2m} \cos(2m\theta)\right] \tag{5.26}$$

$$C_m(\theta) = \overline{C}_m - \frac{2R_m}{\pi^2 \cos\theta}\left[\sum_{n=1}^{\infty} A_{2n} \sin(2n\theta) + \sum_{m=1}^{\infty} B_{2m+1} \cos[(2m+1)\theta]\right] \tag{5.27}$$

For this case, Z was equal to 6 for both expressions. The derivation for this case is contained in Appenkdix 8.2.

$U_o < U_1$ Case

For the case where the maximum oscillatory velocity is greater than the mean, the velocity is negative through part of the cycle, and the representative waveform was asymmetric. Therefore, it is difficult to remove the absolute value term from Equation (5.10). Because of this restriction, expressions for the instantaneous values of the drag and mass coefficients were not derived. The derivation of the expressions for the average values of C_d and C_m is contained in Appendix 8.2, and the results are given here:

$$\overline{C_d} = A_o \left[R_o^2 + \frac{R_1^2}{2} \; 1 + \frac{(\theta_1 - \theta_2)}{\pi} + \frac{2 R_o R_1}{\pi} (\cos \theta_2 - \cos \theta_1) + \frac{R_1^2}{4\pi} (\sin[2\theta_2] - \sin[2\theta_1]) \right]^{-1} \tag{5.28}$$

$$\overline{C_m} = \frac{2K^*}{\pi^2} \left[B_1 + \frac{\overline{C_D}}{\pi} (R_o^2 (\sin \theta_2 - \sin \theta_1) + R_o R_1 (\sin^2 \theta_2 - \sin^2 \theta_1) + \frac{R_1^2}{3} (\sin^3 \theta_2 - \sin^3 \theta_1) \right] \tag{5.29}$$

where

$$\theta_1 = \pi + \sin^{-1} \frac{U_o}{U_1}$$

$$\theta_2 = 2\pi - \sin^{-1} \frac{U_o}{U_1}$$

5.5 Mean Velocity Measurement

As pointed out in the introduction, the model for a drag-force current meter used to take field measurements is usually considered to include only the steady-flow, profile drag term in Equation (1.1). In that case, the force waveform would be described:

$$F^*(\theta) = \frac{C_{ds}\ U^*(\theta)\ |U^*(\theta)|}{2(U_o + U_1)^2} \tag{5.30}$$

where

U^* = measured velocity given F^* as an input

The measured velocity under this assumption is then given by:

$$U^* = \mp \left[(U_o + U_1)^2 \left(\frac{2F^*}{C_{ds}}\right) \right]^{1/2} \tag{5.31}$$

For a representative waveform containing N data points, the ratio of the measured mean velocity to the known input mean is approximated by:

$$\frac{\overline{U^*}}{U_o} = \left(\frac{2}{C_{ds}}\right)^{1/2} \left[1 + \frac{U_1}{U_o}\right] \overline{\overline{F}}_{SQ} \tag{5.32}$$

where

$$\overline{\overline{F}}_{SQ} = \frac{1}{N} \sum_{I=1}^{N} \mp (F^*(I))^{1/2} \tag{5.33}$$

Table 5.4 gives the value of this ratio for each run.

Table 5.4. Mean Velocity Measurement Accuracy

Run No.	U^*/U_o	K*
7	0.864	29.939
8	0.848	64.360
9	0.972	207.287
10	0.631	27.820
11	1.016	142.179
12	0.960	234.629
13	0.401	10.384
14	0.425	17.039
15	0.955	53.951
16	1.098	58.994
17	1.028	168.106
18	0.358	10.512
19	0.,966	27.545
20	1.011	106.151
21	0.895	37.523
22	1.058	109.145
23	1.018	443.331
24	0.949	4.615
25	0.739	7.228
26	0.665	14.013

6. RESULTS AND DISCUSSION

6.1. Meaning of K*

The extended period parameter, K*, is proportional to the ratio of the maximum profile drag to the maximum unsteady inertial force that occurs in the velocity cycle. The maximum profile drag is the first term in Equation (1.1) evaluated at the peak of the sinusoidal flow:

$$F_{FD} = \frac{C_D}{2} \rho D^2 (U_o + U_1)^2 \tag{6.1}$$

The maximum inertial force is the second term in Equation (1.1) evaluated at the point in the velocity cycle where the unsteady component is zero:

$$F_I = \frac{C_m \rho \pi D^3}{4} \left[\frac{2\pi U_1}{T}\right] \tag{6.2}$$

The ratio of the two components is thus:

$$\frac{F_{FD}}{F_I} = \frac{C_D}{C_m \pi^2} \left(\frac{U_1 T}{D}\right) \left[\frac{U_o}{U_1} + 1\right]^2 = \frac{C_D}{C_m \pi^2} K^* \tag{6.3}$$

K* is therefore a measure of the relative magnitudes of the two components evaluated at their respective maximums. At low values of K*, the inertial force makes up a large fraction of the total force on the plate. In this case, the response of lthe sensor is largely a reflection of the acceleration in the flow field. At values of K* greater than about 30, the square term in the profile drag expression begins to dominate and the sensor responds primarily to velocity.

6.2. Instantaneous Values of C_d and C_m

Figures 6.1 through 6.9 contain three examples of representative waveforms and the time variations in C_d and C_m that were derived through Fourier analysis from these waveforms. The representative waveforms show the variation in the measured hydrodynamic force coefficient throughout the period

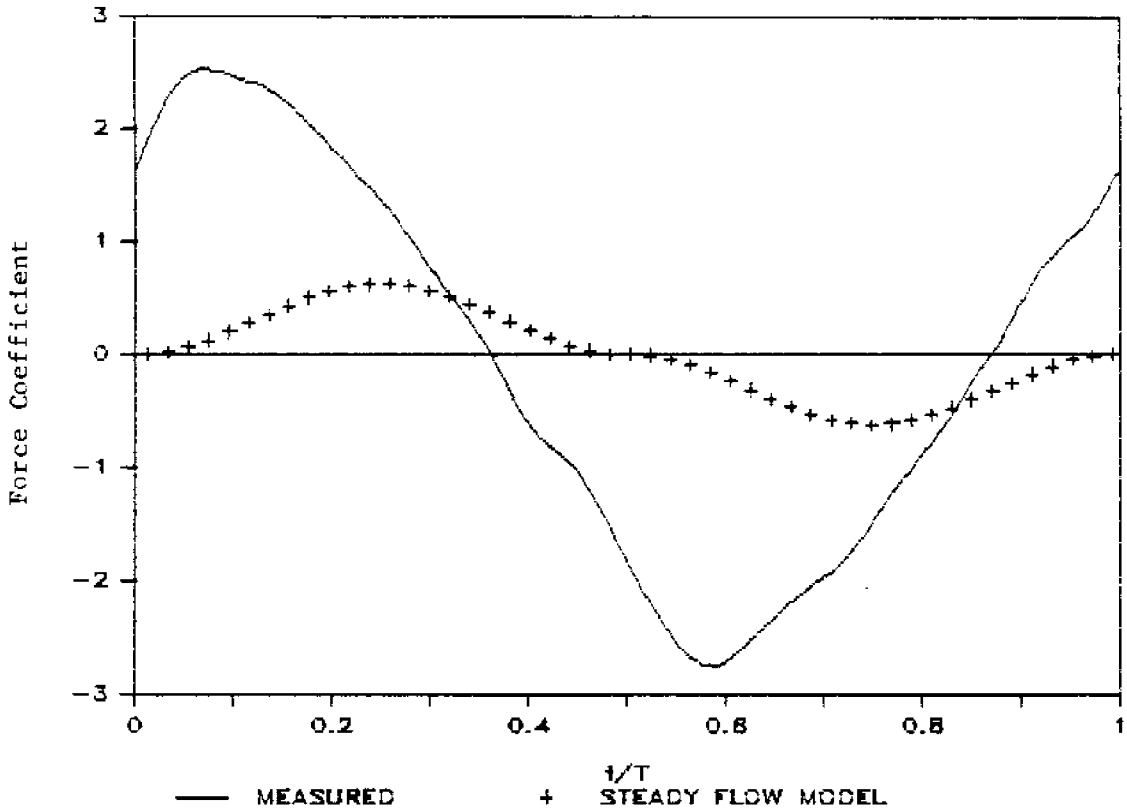

Figure 6.1. Representative Waveform for Run Number 4

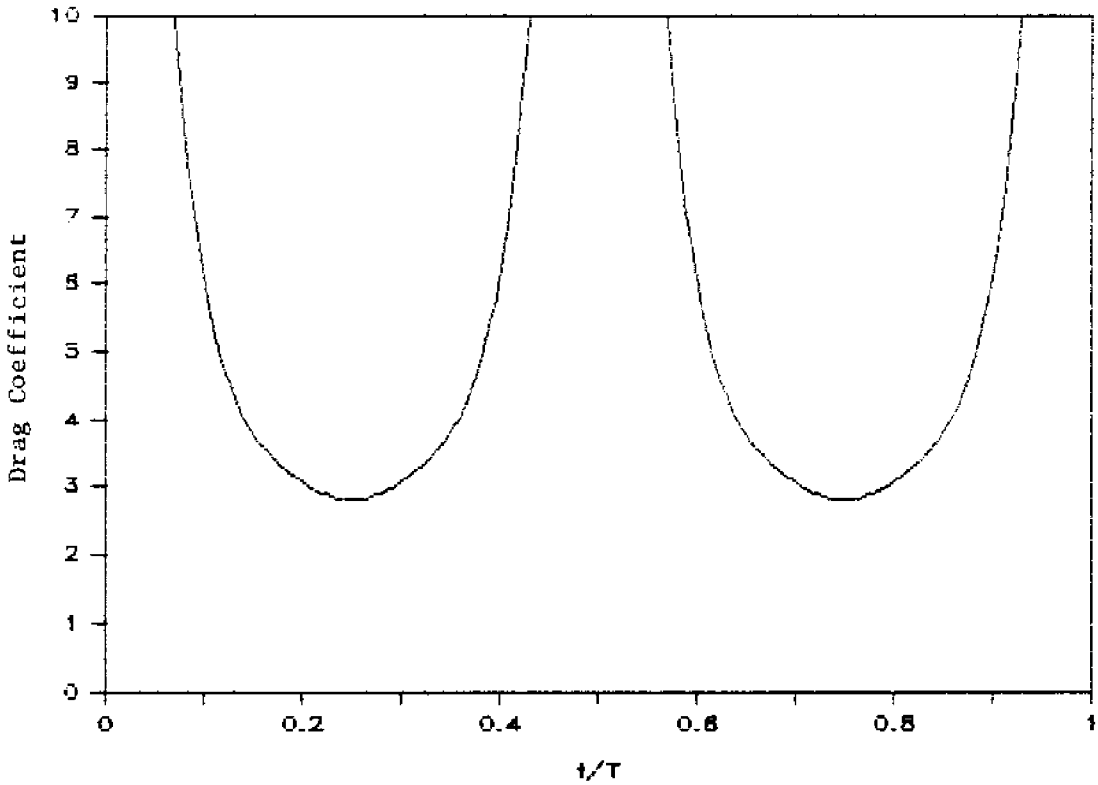

Figure 6.2. Instantaneous Values of C_d for Run Number 4

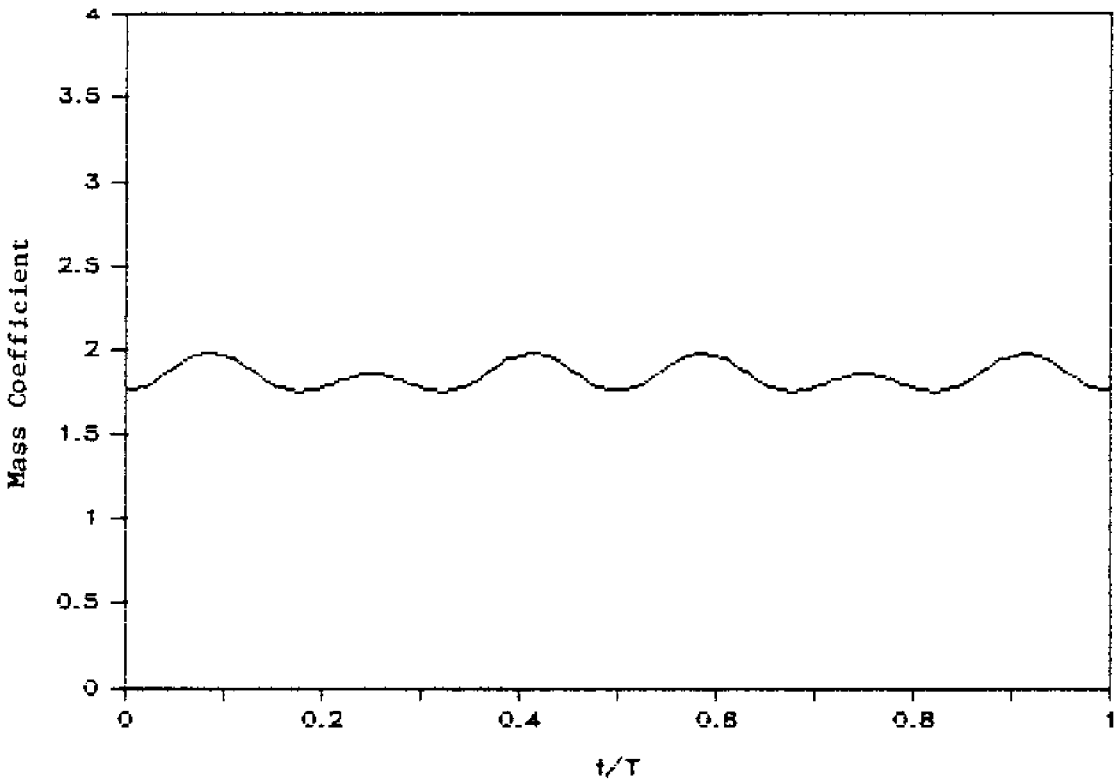

Figure 6.3. Instantaneous Values of C_m for Run Number 4

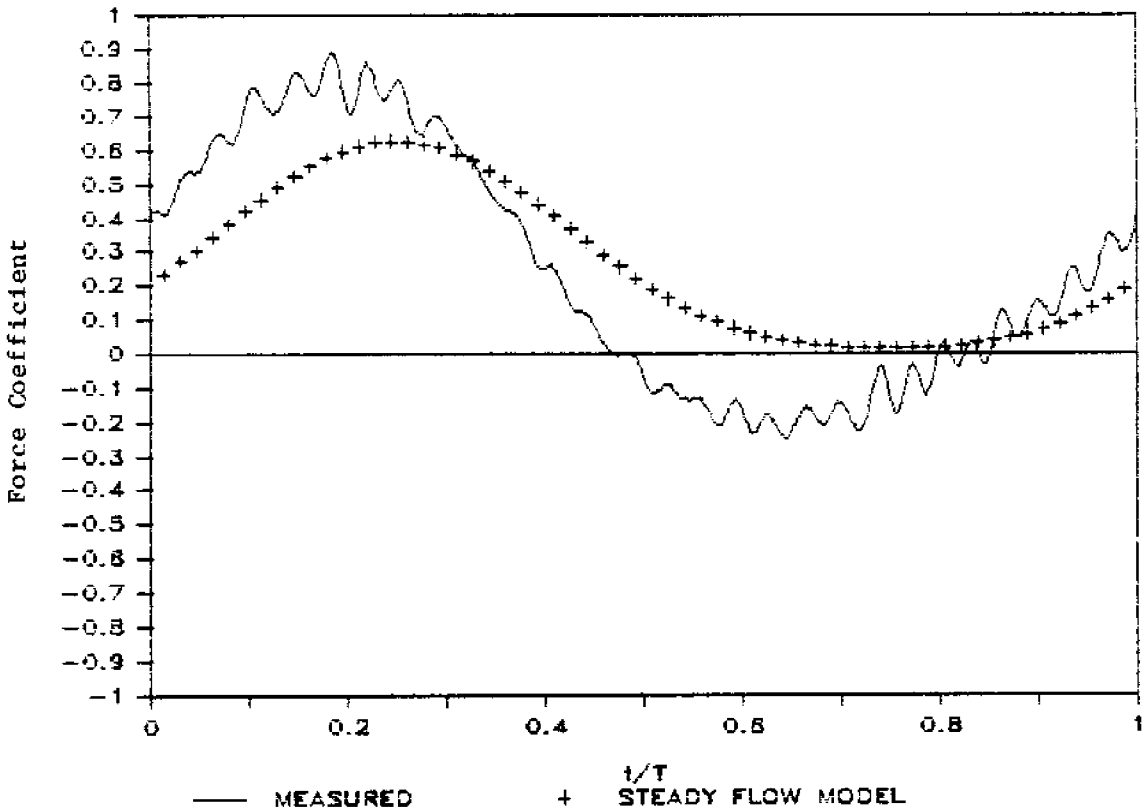

Figure 6.4. Representative Waveform for Run Number 10

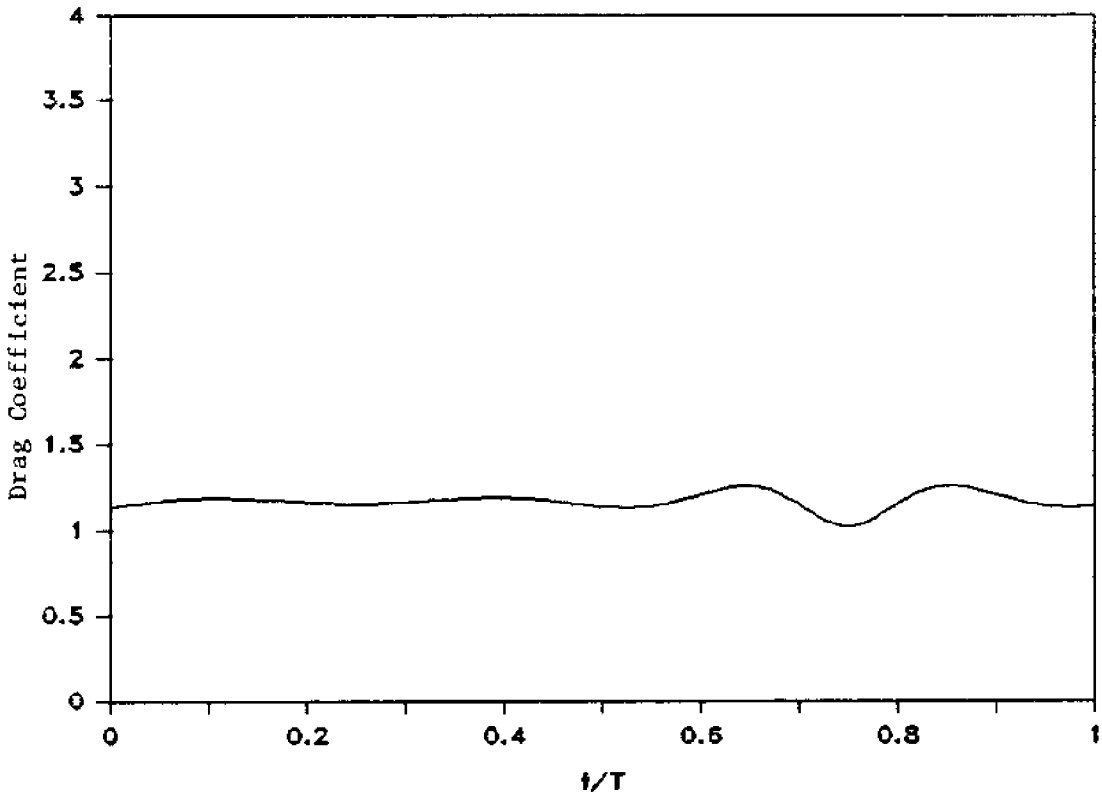

Figure 6.5. Instantaneous Values of C_d for Run Number 10

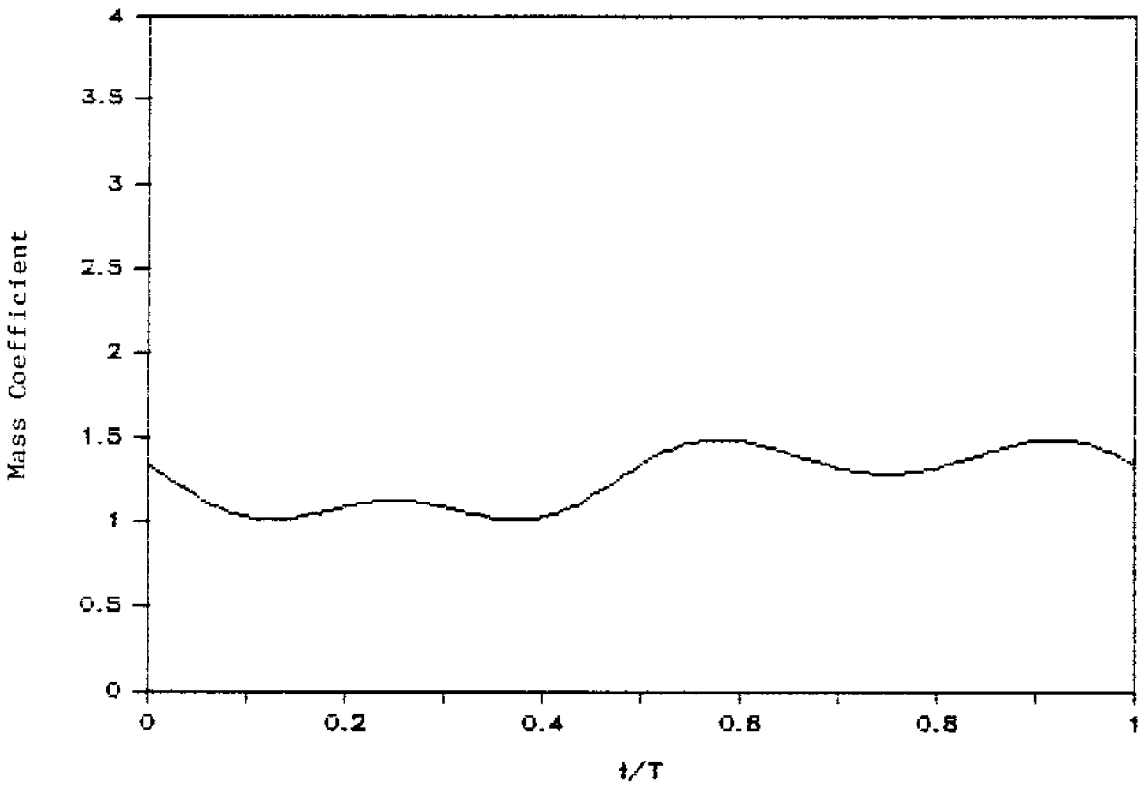

Figure 6.6. Instantaneous Values of C_m for Run Number 10

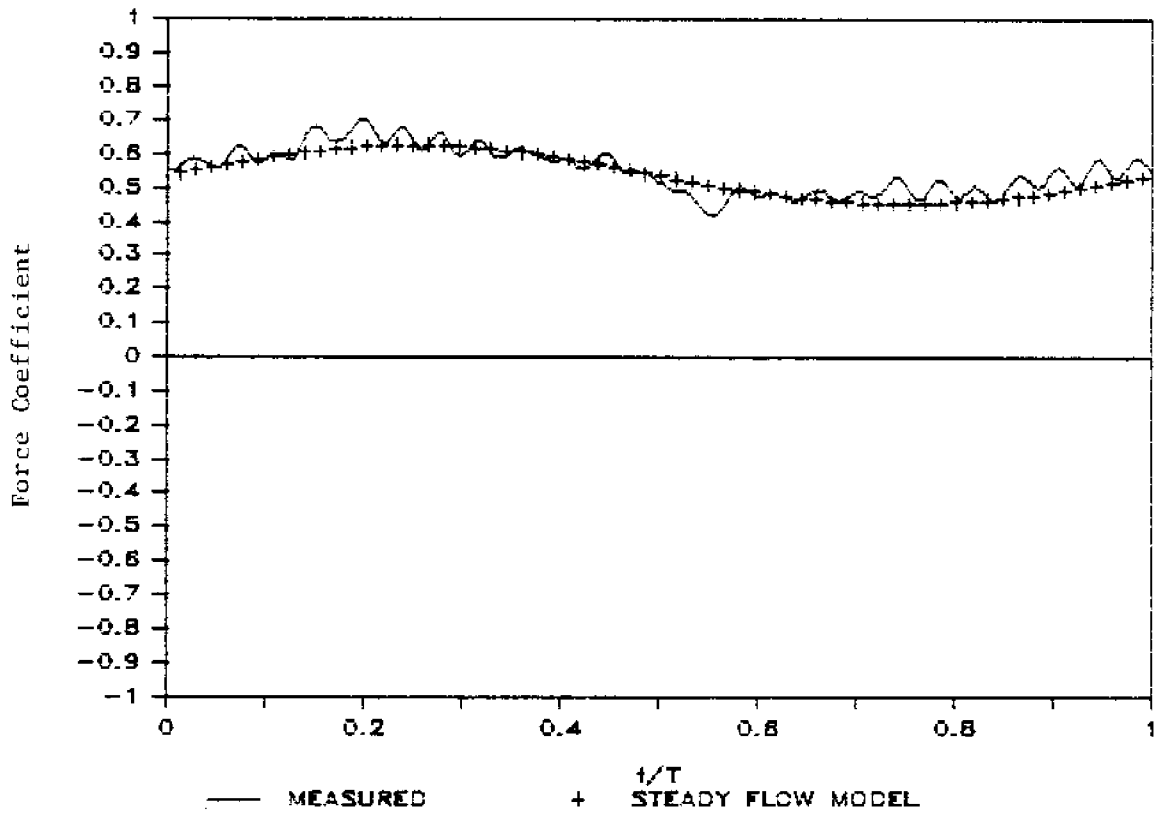

Figure 6.7. Representative Waveform for Run Number 23

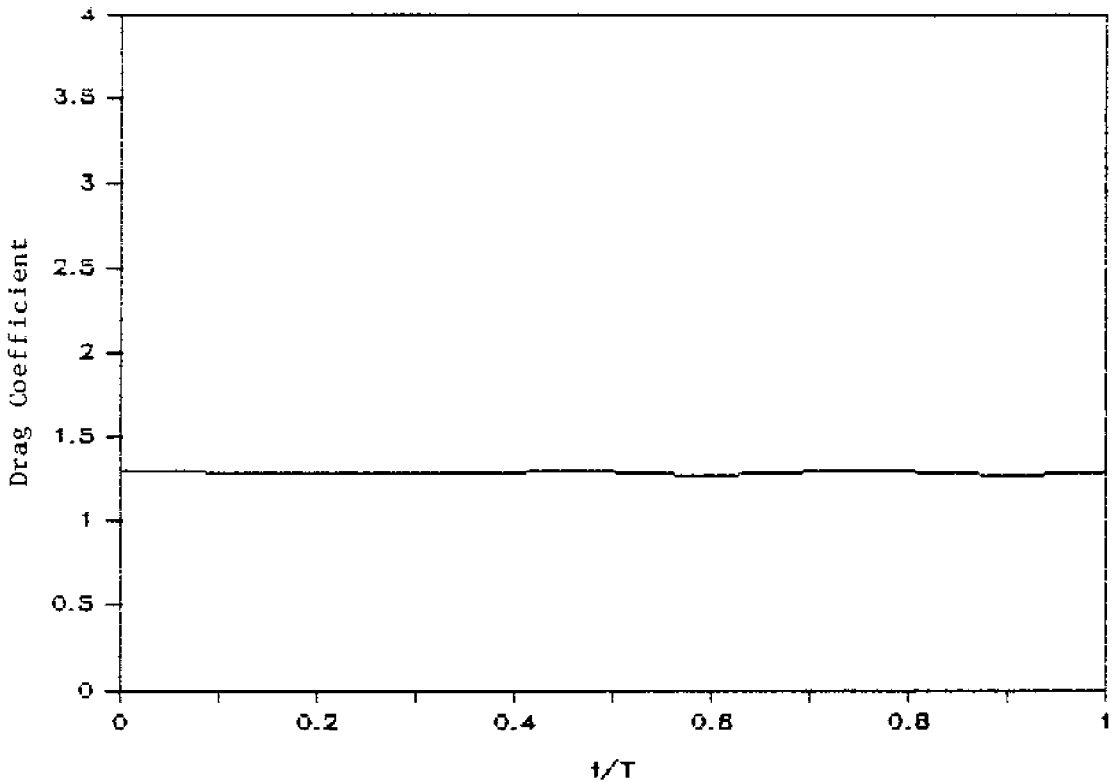

Figure 6.8. Instantaneous Values of C_d for Run Number 23

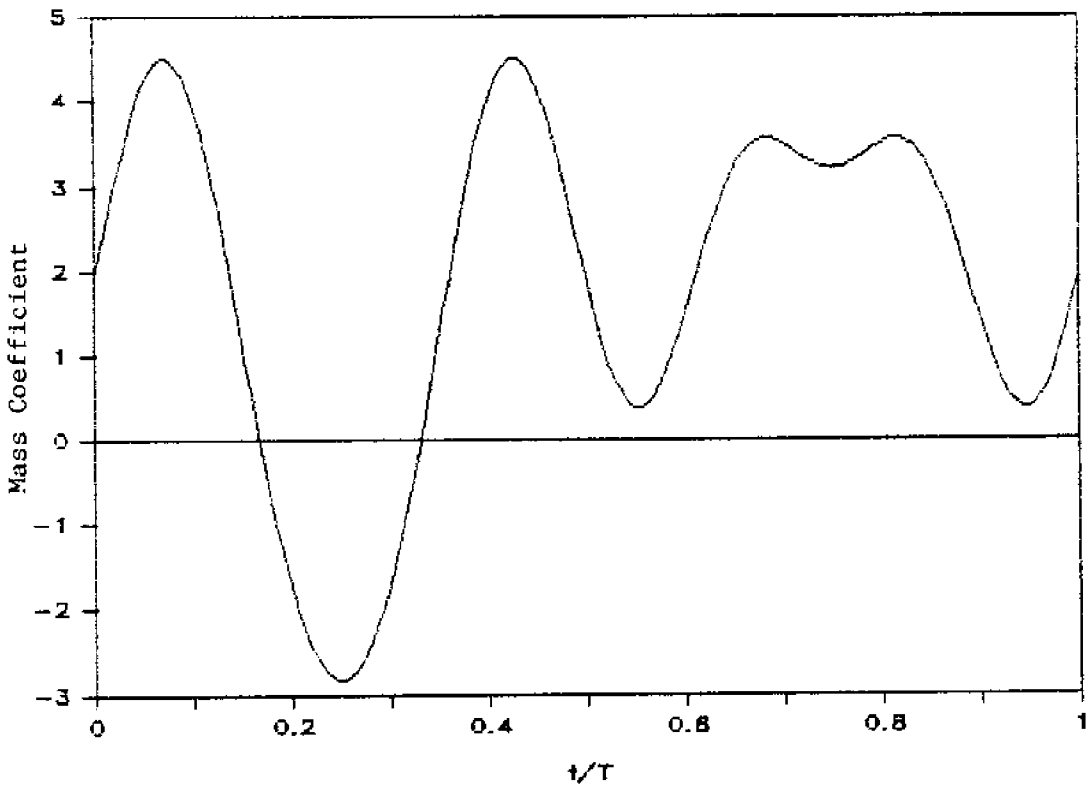

Figure 6.9. Instantaneous Values of C_m for Run Number 23

of the sinusoidal motion cycle of the sensor. Included in these graphs are the predicted variations in the force coefficient calculated using the steady flow model, Equation (5.30).

Figure 6.1 shows the variation in the force coefficient for run #4 and is exemplary of those runs which had a zero mean flow. The force is much greater than that predicted by the simple, steady-flow model and the maximum force leads the maximum velocity in time. As Keulegan and Carpenter found, the values of C_d and C_m are not constant throughout a sinusoidal period with zero mean. The present study yielded results that show a similar character in the time variations. Figures 6.2 and 6.3 are graphs of the cyclic variation of C_d and C_m, respectively, for run #4 and are typical of the behavior of the coefficients for a zero mean flow. C_d tends to a very large value at the points in the waveform where the input velocity is zero. The smallest value is obtained where the velocity is a maximum, but this value is still much greater than the steady flow value. The variations in C_m are continuous and much smaller in magnitude than those of C_d.

Figures 6.4 through 6.6 are from run #10 which was typical of runs with values of K* in the range of 10 to around 30. Vibration from the cart used to generate the mean flow is apparent in the graph. The steady-flow model again underestimates the maximum force and the maximum force again leads the maximum velocity in time. With the introduction of a mean velocity, the character of the time variations in C_d and C_m changes dramatically. C_d is now constant through most of the period. Figure 6.6 shows the singular variations in C_m that are typical of runs in this range.

Figures 6.7 through 6.9 are from run #23 which has the largest value of K* obtained in this experiment. Steady flow tends to dominate the dynamics of this situation and thus the steady flow model predicts the maximum force with better accuracy. As would be expected, the phase difference is also smaller than that found at lower values of K*. C_d is continuous throughout the cycle and similar in character to the mass coefficient for the zero mean-flow runs. The large variation in C_m shown in Figure 6.9 correspond to the points in the period where the acceleration is zero. The character of the coefficients of runs with large K* is therefore seen to be the reverse of that found for zero mean-flow runs, all of which have small values of K*. Recall that a large value of K* denotes a flow in which the hydrodynamic force is dominated by profile drag, whereas in a flow with a small value of K* the inertial force dominates.

6.3 Average Values of C_d and C_m

Figure 6.10 is a plot of $\overline{C_d}$ versus K* for the zero mean flow runs from the present study and from the data of Keulegan and Carpenter. Recall that for a zero mean oscillation, K* reduces to the period parameter, K. Both studies yielded values of the coefficient that are greater than the published value of 1.17 for a square plate. The results of the present study, while similar in form to the previous work, indicate smaller values of C_d. One possible explanation for the difference is that the present study used a square plate, whereas the previous experiment was performed with a plate that

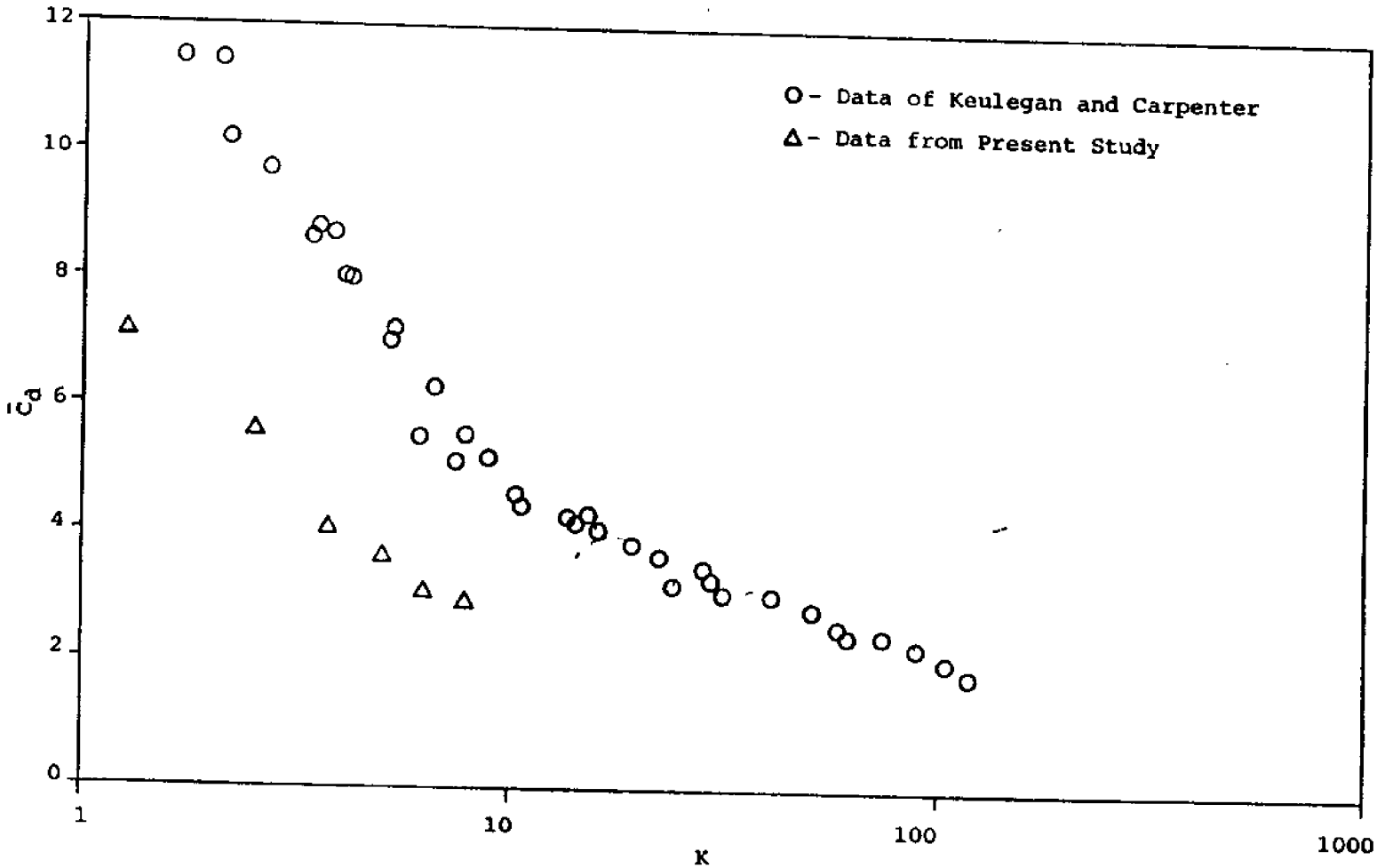

Figure 6.10. Cycle Averaged Drag Coefficient for Zero Mean Velocity

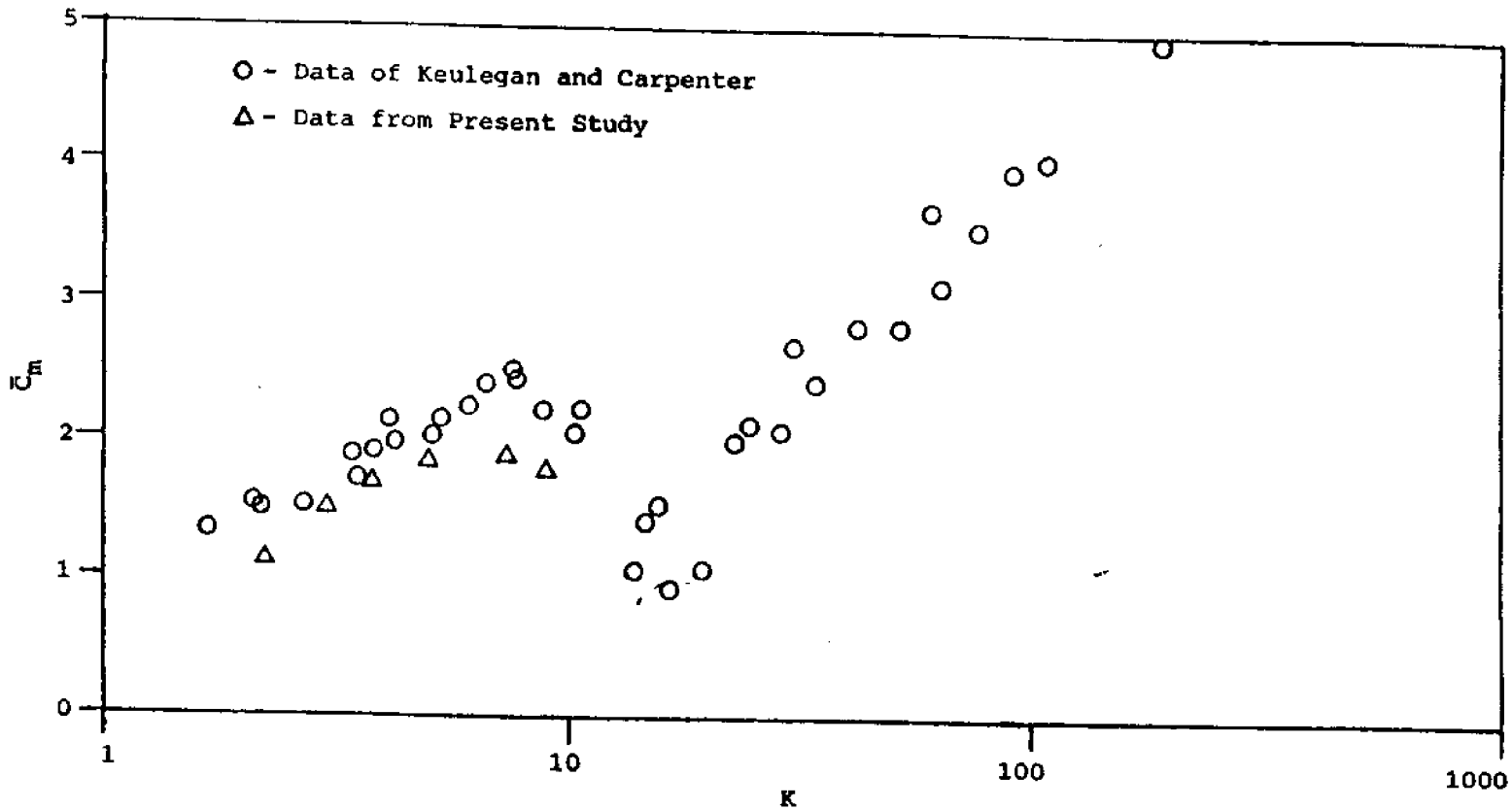

Figure 6.11. Cycle Averaged Mass Coefficient for Zero Mean Velocity

spanned the test channel, thus approximating two-dimensional flow. The value of the steady-flow drag coefficient (10) for two-dimensional flow around a flat plate (approximately 2) is larger than the value for three-dimensional flow around a square plate (1.17). Such a difference also appears to exist in unsteady flow.

The values of $\overline{C_m}$ from the two studies are plotted against K* in Figure 6.11. The two data sets correlate well for this coefficient. There has been some discussion of hydrodynamic differences that may exist between the flow caused by oscillating the fluid about the body, and oscillating the body in a still fluid. Some investigators (9) have suggested that this difference would be seen as a difference in the value of $\overline{C_m}$ for the two situations. Figure 6.11 suggests no such difference since the two data sets are products of the two different situations.

Figures 6.12 and 6.13 show the correlation of the cycle average values of C_d and C_m with the extended period parameter for both zero and non-zero mean velocity flow. Figure 6.12 is a plot of $\overline{C_d}$ versus K* for the three cases described in Section 5.3. There is a discontinuity between the values obtained from the zero mean flow case and the other two cases. This discontinuity indicated that the existence of a mean flow causes a reduction in the profile drag. The two non-zero mean-flow cases produced similar values of $\overline{C_d}$ over the range of K* in which they overlapped. Both cases showed a dip in the value of the drag coefficient over that range as compared to higher values of K*. For values of K* greater than 25, $\overline{C_d}$ seems to attain a constant value. The average of the 14 values of $\overline{C_d}$ for K* greater than 25 is 1.287 with a standard deviation of 0.098. This value is 3% greater than the steady-flow value of 1.25 that was obtained during the experiment. This percentage difference is considered to be within experimental error.

Figure 6.13 is a plot of $\overline{C_m}$ for the three cases. The scatter in this coefficient is larger than that for $\overline{C_d}$. This observation indicates that vibration from the carriage used to produce the mean velocity probably is the source of error in the experiment and that the vibration most strongly affects the mass coefficient. The most scatter occurred for the $U_o < U_1$ case. There is no apparent discontinuity in $\overline{C_m}$ between the zero and non-zero mean-flow cases. The graph indicated an increase in the value of $\overline{C_m}$ for K* greater than 25. Unlike the drag coefficient, a trend toward a constant value could not clearly be established, although the range of values of $\overline{C_m}$ was smaller than that of $\overline{C_d}$.

6.4 Usefulness of the Flat Plate Current Meter

If a drag-force current meter is to be useful in unsteady nearshore flows, it must be used in a flow regime in which the steady flow model will correctly predict the velocity. Implicit in this requirement is the need for a constant drag coefficient which is nearly equal to the steady-flow drag coefficient so that complex, unsteady-flow calibrations are avoided. The extended period parameter provides one way of quantifying that regime. Plots of the variation of C_d throughout the velocity cycle indicate that the coefficient becomes constant as K* increases. Figure 6.12 shows that for values of K* greater than 25, the average drag coefficient is constant and has a value which is equal to the steady-flow value within experimental error.

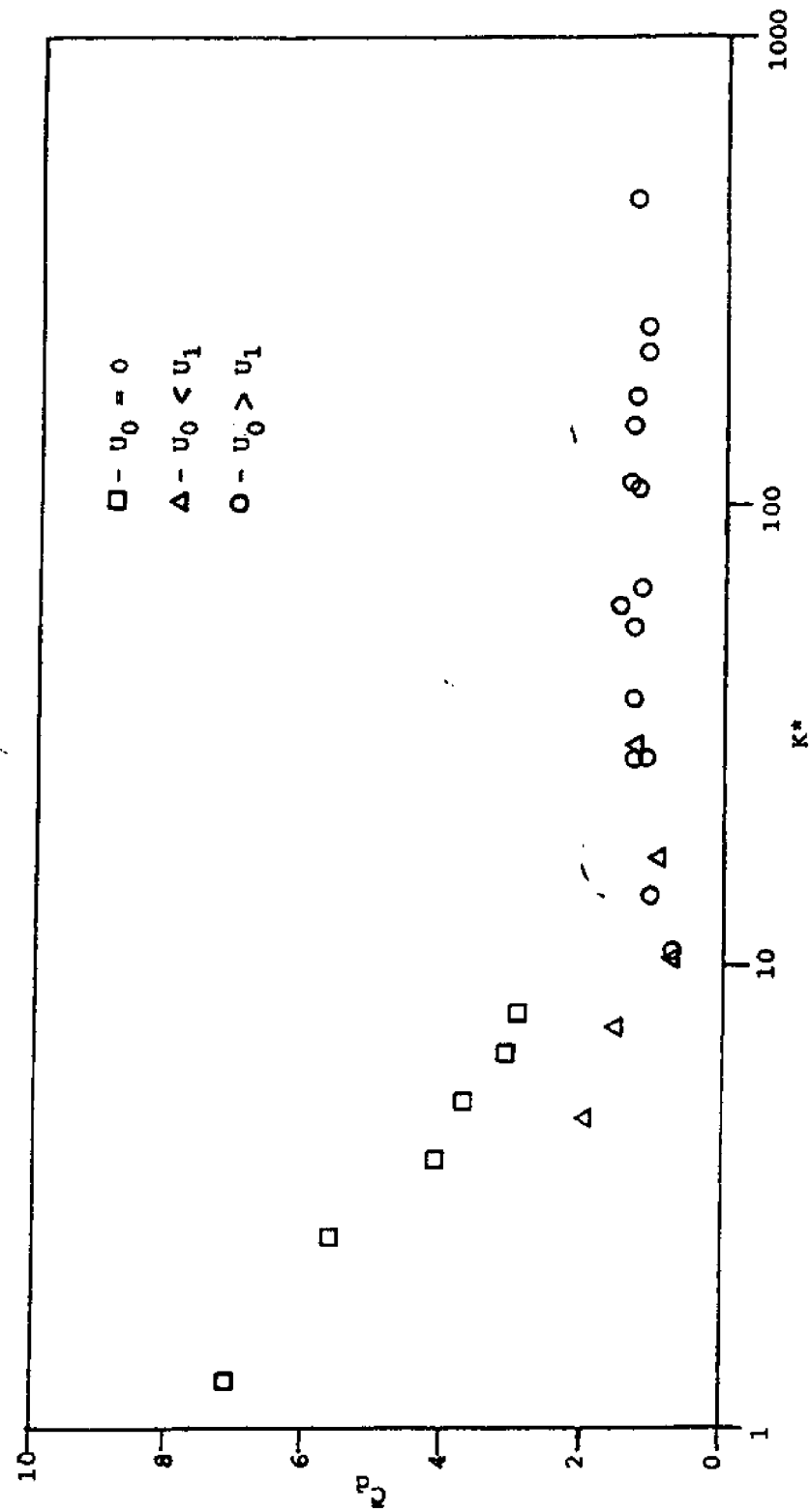

Figure 6.12. Cycle Averaged Drag Coefficient

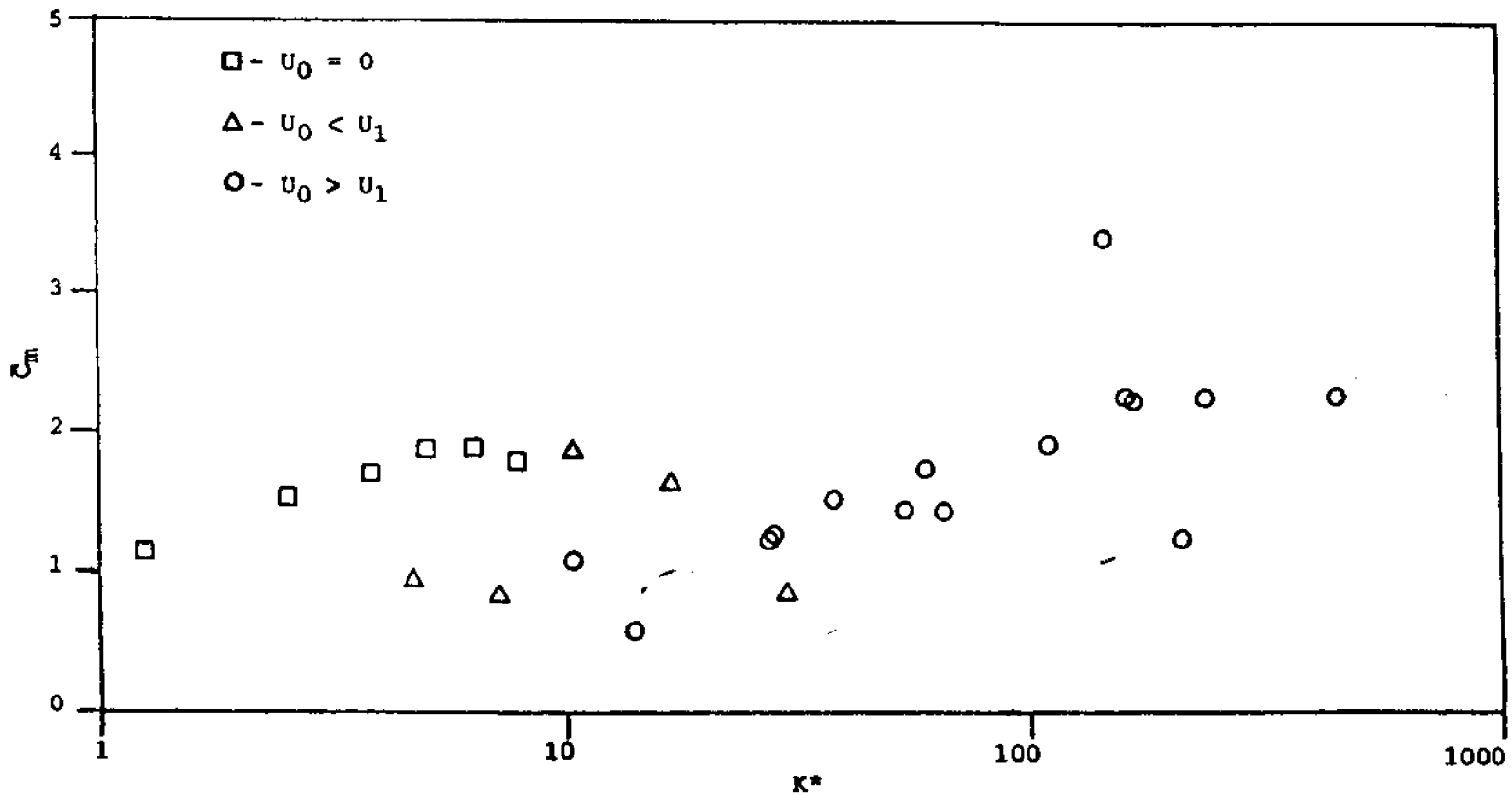

Figure 6.13. Cycle Averaged Mass Coefficient

This steady-flow value was 6.8% higher than the published value for a flat plate. The probable explanation for this difference is the partial blocking on the upper side of the plate caused by the top portion of the aluminum frame.

The results concerning the constancy and predictability of the drag coefficient indicate that the extended period parameter is useful in determining those flow fields in which the flat-plate current meter can be used with acceptable accuracy. To reinforce this conclusion the ability of the sensor to accurately measure the mean velocity in an unsteady flow is shown as a function of K* in Figure 6.14. For values of K* greater than 50, the error in mean velocity measurement is typically less than 10%, and is less than 6% for K* greater than 100. As an example, a K* of 50 is produced for the 12.7 cm by 12.7 cm plate by an oscillatory velocity of 5 cm/sec, a mean velocity of 15 cm/sec and a period of 8 sec. For flows with a K* less than 50 the sensor underestimated the mean velocity.

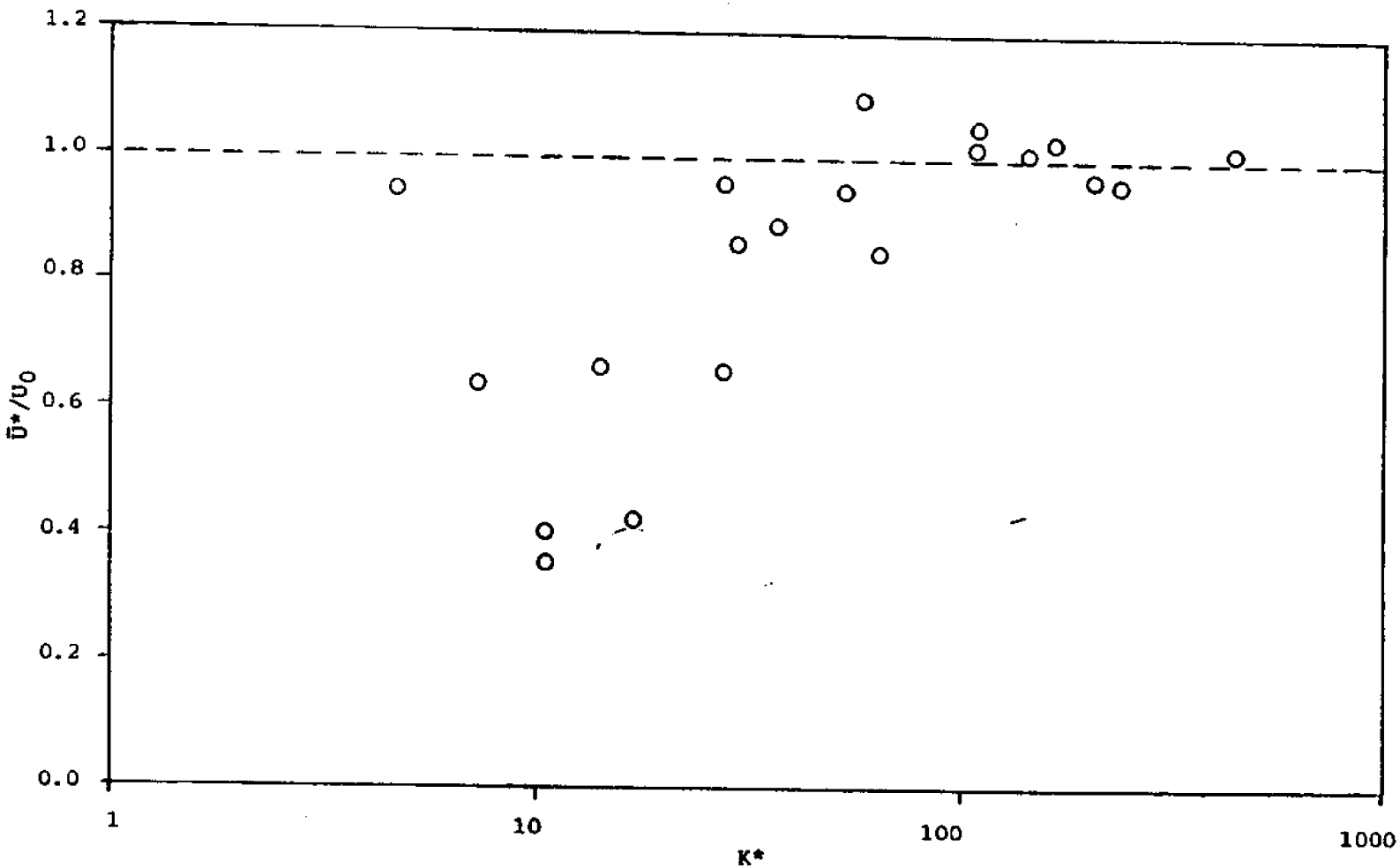

Figure 6.14. Accuracy of Mean Velocity Measurement

7. LIST OF REFERENCES

1. O'Brien, M. P. and J. R. Morison. 1952. "The Forces Exerted by Waves on Objects," Amer. Geophy. Union Trans., 33:32-38.

2. Inman, D. L. and N. Nasu. 1956. Orbital Velocity Associated with Wave Action Near the Breaker Zone. Corps of Engineers, Beach Erosion Board, Technical Memo No. 79:1-43.

3. Beardsley, G. P., Jr., G. C. Knollman, A. S. Hamamoto, and J. D. Eisler. 1963. "A Device for Measuring Orbital Velocities in an Underwater Wave Field." Rev. Sci. Insts., 34:516-519.

4. Smith, D. and W. Harrison. 1970. "Water Current Meter for Mean Flow Measurement." Proc. 12th Coastal Engr. Conf., Washington, D. C., pp. 1094-1915.

5. Russell, J. R. 1979. "Drag Force Water Current Meter for Mean or Steady Flow Measurement." Marine Geol., 33:M33-M40.

6. Keulegan, G. H. and L. H. Carpenter. 1958. "Forces on Cylinders and Plates in an Oscillating Fluid." Journal of Research of the National Bureau of Standards, 60:423-440.

7. Olson, J. R. 1967. Flow Meters in Shallow Water Oceanography. Naval Underwater Warfare Center, U. S. Navy, No. TP 5, pp. 1-44.

8. Hoerner, S. P. 1965. Fluid-Dynamic Drag. Published by the author, New Jersey.

9. Mercier, J. A. 1973. Large Amplitude Oscillations of a Circular Cylinder in a Low-Speed Stream. Ph.D. Dissertation, Stevens Institute of Technology.

10. Li, W. and S. Lam. 1976. Principles of Fluid Mechanics. Addison-Wesley Publishing Company, Reading, Massachusetts.

8. APPENDICES

Appendix 8.1

Physical Characteristics of Transducers

Assemblies and Electronics

PLATE

Size: 12.7 cm by 12.7 cm
Material: 0.318 cm thick ABS plastic

FORCE TRANSDUCER

Material: 1.27 cm diameter 6061-T6 aluminum rod
Moment Arm Length: 10.16 cm
Modulus of Elasticity: 6.894×10^{11} dyne/cm^2
Yield Strength: 2.758×10^{9} dyne/cm^2

Two strain gages were mounted on a pair of parallel rectangular flats milled into the rod near the cantilevered end. The flats were 0.762 cm wide. The thickness of the material between the flats was 0.229 cm. The strain gage site was waterproofed by enclosing it in a section of 1.27 cm diameter latex tubing. The tubing was safety wired into grooves milled into the surface of the rod on both ends of the gage site. The volume enclosed by the tubing was filled with glycerin.

STRAIN GAGE

Type: Micromeasurements CEA-125-UW-350
Nominal Resistance: 350 ohms
Nominal Gage Factor: 2.13

WHEATSTONE BRIDGE

Configuration: Half-Bridge, bending stress
Fixed Resistors: (2) 1000 ohm films deposited on the same substrate for temperature compensation
Bridge Supply Voltage: 9 volts
Amplifier Gain: 500

Appendix 8.2

Derivation of the Expressions for the Instantaneous and Average Values of the Drag and Mass Coefficients

The representative waveform for each run was modeled by the nondimensionalized form of Morison's equation (Equation (5.10)):

$$F^*(\theta) = \frac{C_d}{2}(R_o + R_1 \sin\theta)|R_o + R_1 \sin\theta| + \frac{C_m \pi^2}{2K^*}\cos\theta \qquad (8.2.1)$$

This model was equated to a series of lksine and cosine terms (Equation (5.12)):

$$F^*(\theta) = \frac{A_o}{2} + A_1 \sin(\theta) + A_2 \sin(2\theta) + A_3 \sin(3\theta) + \ldots + B_1 \cos(\theta) + B_2 \cos(2\theta) + B_3 \cos(3\theta) + \ldots + \qquad (8.2.2)$$

where:

$$\theta = 2\pi \frac{t}{T}$$

The Fourier coefficients in Equation (8.2.2) are defined:

$$A_o = \frac{1}{\pi}\int_o^{2\pi} F^*(\theta)d\theta \qquad (8.2.3)$$

$$A_n = \frac{1}{\pi}\int_o^{2\pi} F^*(\theta)\sin(n\theta)d\theta \quad n > 1 \qquad (8.2.4)$$

$$B_n + \frac{1}{\pi}\int_o^{2\pi} F^*(\theta)\cos(n\theta)d\theta \quad n > 1 \qquad (8.2.5)$$

Combining Equations (8.2.1) and (8.2.2):

$$\frac{C_d}{2}(R_o + R_1 \sin\theta)R_o + R_1 \sin\theta\,|\,+\frac{C_m\pi^2}{2K^*}\cos\theta$$

$$= \frac{A_o}{2} + A_1 \sin\theta + \sum_{n=2}^{\infty} A_n \sin(n\theta)$$

$$+ B_1 \cos\theta + \sum_{n=2}^{\infty} B_n \cos(n\theta) \qquad (8.2.6)$$

Derivation for $U_o = 0$ Case

For this case:

$$R_o = 0$$

$$R_1 = 1$$

Since the average hydrodynamic force is zero for this case, the representative waveform is symmetric in time:

$$F^*(\theta) = -F^*(\theta + \pi)$$

Therefore, the even Fourier coefficients are zero. Equation (8.2.6) becomes:

$$\frac{C_d}{2}\sin\theta\,|\sin\theta| + \frac{C_m\pi^2}{2K^*}\cos\theta = A_1 \sin\theta$$

$$+ \sum_{n=3,5,7,\ldots}^{\infty} A_n \sin(n\theta) + B_1 \cos\theta$$

$$+ \sum_{n=3,5,7,\ldots}^{\infty} B_n \cos(n\theta) \qquad (8.2.7)$$

$\sin\theta\,|\sin\theta|$ can be expressed as an expansion as:

$$\sin\theta\,|\sin\theta| = D_1 \sin\theta + D_3 \sin(3\theta) + D_5 \sin(5\theta) + \ldots + \qquad (8.2.8)$$

where

$$D_n = 0 \qquad \text{where n is even}$$

$$D_n = \frac{1}{\pi} \int_0^{2\pi} |\sin\theta|(\sin\theta)\sin n\theta \, d\theta$$

$$\text{where n is odd} \qquad (8.2.9)$$

Carrying out the integration for D_1 through D_7 yields:

$$D_1 = \frac{8}{3\pi}$$

$$D_3 = \frac{-8}{15\pi}$$

$$D_5 = \frac{-8}{105\pi}$$

$$D_7 = \frac{-8}{315\pi}$$

Solving the expansion for sin θ yields:

$$\sin\theta = \frac{|\sin\theta| \sin\theta}{D_1} - \frac{D_3}{D_1}\sin(3\theta) - \frac{D_5}{D_1}\sin(5\theta)$$

$$- \frac{D_7}{D_1}\sin(7\theta) - \ldots - \qquad (8.2.10)$$

Substituting the expression for sin θ (Equation (8.2.10)) into Equation (8.2.7) and regrouping yields:

$$\frac{C_d}{2}\sin\theta\,|\sin\theta| + \frac{C_m \pi^2}{2K^*}\cos\theta = \frac{A_1}{D_1}\sin\theta\,|\sin\theta|$$

$$+ \sum_{n=3,5,7,\ldots,}^{\infty} \left[A_n - \frac{D_n}{D_1}A_1\right]\sin(n\theta)$$

$$+ B_1\cos\theta + \sum_{n=3,5,7}^{\infty} B_n\cos(n\theta) \qquad (8.2.11)$$

The average values of the drag and mass coefficients, $\overline{C_d}$ and $\overline{C_m}$, are found by assuming that Morison's equation (Equation (8.2.1)) holds exactly with constant coefficients. Under this assumption, all the terms on the right-hand side of Equation (8.2.11) vanish except for two terms:

$$\frac{C_d}{2} \sin\theta\,|\sin\theta| + \frac{C_m \pi^2}{2K^*} \cos\theta = \frac{A_1}{D_1} \sin\theta\,|\sin\theta| + B_1 \cos\theta \qquad (8.2.12)$$

Therefore, the average values of the drag and mass coefficients are given by:

$$\overline{C_d} = \frac{2A_1}{D_1} \qquad (8.2.13)$$

$$\overline{C_m} = \frac{2K^*B_1}{\pi^2} \qquad (8.2.14)$$

Equation (8.2.1) can be forced to fit the representative waveform by allowing the drag and mass coefficients to vary. The expressions for the variable coefficients, $C_d(\theta)$ and $C_m(\theta)$, are obtained by including the terms that were assumed to be zero for the constant coefficient case. From Equation (8.2.11):

$$\frac{C_d(\theta)}{2} \sin\theta\,|\sin\theta| = \frac{A_1}{D_1} \sin\theta\,|\sin\theta| + \sum_{n=3,5,7,\ldots}^{\infty} \left[A_n - \frac{D_n}{D_1} A_1\right] \sin(n\theta) \qquad (8.2.15)$$

$$\frac{C_m(\theta)\pi^2}{2K^*} \cos\theta = B_1 \cos\theta + \sum_{n=3,5,7}^{\infty} B_n \cos(n\theta) \qquad (8.2.16)$$

Recalling the expression for the average coefficients, the instantaneous expressions are:

$$C_d(\theta) = \overline{C_d} + \frac{2}{\sin\theta\,|\sin\theta|} \sum_{n=3,5,7}^{\infty} \left[A_n - \frac{D_n}{2} \overline{C_d}\right] \sin(n\theta) \qquad (8.2.17)$$

$$C_m(\theta) = \overline{C_m} + \frac{2R_m}{\pi^2 \cos\theta} \sum_{n=3,5,7,\ldots}^{\infty} B_n \cos(n\theta) \qquad (8.2.18)$$

Derivation for $U_o > U_1$

For this case if is convenient to represent the velocity as

$$U = U_o + U_1 \cos\theta' \qquad (8.2.19)$$

comparing to Eq. 7.

$$\theta' = \theta - \pi/2 \qquad (8.2.20)$$

and

$$F^*(\theta) = \frac{C_d}{2} (R_o + R_1 \cos\theta') \left| R_o + R_1 \cos\theta' \right| - \frac{C_m \pi^2}{2R_m} \sin\theta' \qquad (8.2.21)$$

For $U_o < U_1$

$$F^*(\theta) = \frac{C_d}{2} (R_o^2 + 2R_o R_1 \cos\theta' + R_1^2 \cos^2\theta') - \frac{C_m \pi^2}{2R_m} \sin\theta' \qquad (8.2.22)$$

Using $\cos^2\theta' = 1/2 + 1/2 \cos(2\theta')$

$$F^*(\theta) = \frac{C_d}{2} \left[R_o^2 + \frac{R_1^2}{2} 2R_o R_1 \cos\theta' + \frac{R_1^2}{2} \cos(2\theta)'\right] - \frac{C_m \pi^2}{2R_m} \sin\theta' \qquad (8.2.23)$$

A new fourier expansion is now made in θ'

$$F^*(\theta) = \frac{B_o'}{2} + \sum_{m=1}^{\infty} B_m' \cos(m\theta') + \sum_{n=1}^{\infty} A_n' \sin(n\theta') \qquad (8.2.24)$$

The (primed) coefficients in this expansion can be related to the (unprimed) coefficients in the original expansion given by Eq. (8.2.2)

$$B_o' = A_o$$

$$B_m' = (-1)^{\frac{m-1}{2}} A_m \qquad m \text{ odd}$$

$$B_m' = (-1)^{\frac{m}{2}} B_m \qquad m \text{ even} \tag{8.2.25}$$

$$A_n' = (-1)^{\frac{n+1}{2}} B_n \qquad n \text{ odd}$$

$$A_n' = (-1)^{\frac{n}{2}} A_n \qquad n \text{ even}$$

These will be used later. Equating Eq. 8.2.23 to 8.2.24 gives

$$\frac{Cd}{2}\left[R_o^2 + \frac{R_1^2}{2} + 2R_oR_1\cos\theta' + \frac{R_1^2}{2}\cos(2\theta') - \frac{C_m\pi^2}{2R_m}\sin\theta'\right.$$

$$= \frac{B_o'}{2} + B_1'\cos\theta' + B_2'\cos(2\theta) + \sum_{m=3}^{\infty} B_m'\cos(n\theta')$$

$$\left. + A_1'\sin\theta' + \sum_{n=2}^{\infty} A_n'\sin(n\theta')\right. \tag{8.2.26}$$

If Morison's equation (Eq. 4) held for constant values of D_d & C_m, e.g., $\overline{C_d}$ & $\overline{D_m}$ then.

$$\frac{B_o'}{2} = \frac{\overline{C}_d}{2}\left(R_o^2 + \frac{R_1^2}{2}\right) \tag{8.2.27a}$$

$$B_1' = \frac{\overline{C}_d}{2}(2R_1R_o) \tag{8.2.27b}$$

$$B_2' = \frac{\overline{C}_d}{2} \frac{R_1^2}{2} \tag{8.2.27c}$$

$$A_1' = -\frac{C_m \pi^2}{2R_m} \tag{8.2.27d}$$

Rearranging

$$\overline{C}_d = \frac{B_o'}{R_o^2 + \frac{R_1^2}{2}} = \frac{A_o}{R_o^2 + \frac{R_1^2}{2}} \tag{8.2.28}$$

Equations (8.2.27) and (8.2.27c) can be used as a check on $\overline{C_d}$. In order to develop a consistent expansion they are left as is:

$$B_1' = R_o R_1 \overline{C}_d \tag{8.2.29a}$$

$$B_2' = \frac{R_1^2 \overline{C}_d}{4} \tag{8.2.29b}$$

and

$$\overline{C}_m = \frac{2R_m}{\pi^2} A_1' = \frac{2R_m}{\pi^2} B_1 \tag{8.2.30}$$

Eq.'s (8.2.28) and (8.2.30) thus give the time average values, $\overline{C}_d$ & $\overline{C}_m$. (With a check on $\overline{C}_d$ provided by (8.2.29). They are written in terms of the original expansion (Eq. 8.2.2). In order to obtain the instantaneous values, $C_d(\theta)$ and $C_m(\theta)$, the higher order terms in the expansion are included.

$$\frac{C_d}{2}\left[R_o^2 + \frac{R_1^2}{2} + 2R_o R_1 \cos\theta' + \frac{R_1^2}{2}\cos(2\theta')\right] - \frac{C_m \pi^2}{2R_m} \sin '$$

$$= \frac{\overline{C}_d}{2}\left[R_o^2 + \frac{R_1^2}{2} + 2R_o R_1 \cos\theta' + \frac{R_1^2}{2}\cos(2\theta')\right] + \sum_{m=3}^{\infty} B_m' \cos(m\theta')$$

$$- \frac{C_m \pi^2}{2R_m} \sin\theta' + \sum_{A=2}^{\infty} A_n' \sin(n\theta') \qquad (8.2.31)$$

Thus

$$\overline{C}_d(\theta') = \overline{C}_d + \frac{2}{R_o^2 + \frac{R_2^2}{2} + 2R_oR_1 \cos\theta' + \frac{R_1^2}{2}\cos(2\theta')} \sum_{m=3}^{\infty} B_m' \cos(m\theta') \qquad (8.2.32)$$

Using the original trigonometric identity one can show

$$R_o^2 + \frac{R_1^2}{2} + 2R_oR_1 \cos\theta' + \frac{R_1^2}{2}\cos(2\theta') = (R_o + R_1 \cos\theta')^2 \qquad (8.2.33)$$

Thus

$$C_d(\theta') = \overline{C}_d + \frac{2}{(R_o + R_1 \cos\theta')^2} \sum_{m=3}^{\infty} B_m' \cos(m\theta') \qquad (8.2.34)$$

$$C_m(\theta') = \overline{C}_m - \frac{2R_m}{\pi^2 \sin\theta'} \sum_{n=2}^{\infty} A_n' \sin(n\theta') \qquad (8.2.35)$$

Note that as long as

$$\frac{R_o}{R_1} = \frac{U_o}{U_1} > 1 \qquad (8.36)$$

Both $C_d(\theta')$ & $C_m(\theta')$ remain bounded.
For convenience in computation Eq.'s (8.2.34) and 8.2.35) are written in the original variable, θ'.

$$C_d(\theta) = \overline{C}_d + \frac{2}{(R_o + R_1 \sin\theta)^2} \left[\sum_{n=1}^{\infty} A_{2n+1} \sin[(2n+1)\theta] + \sum_{m=2}^{\infty} B_{2m} \cos(2m\theta) \right] \qquad (8.2.37)$$

$$C_m(\theta) = \overline{C}_m - \frac{2R_m}{2\cos\theta}\left[\sum_{n=2}^{\infty} A_{2n}\sin(2n\theta) + \sum_{m=1}^{\infty} B_{2m+1}\cos[(2m+1)\theta]\right] \qquad (8.2.38)$$

Because the coefficients A_n and B_m have already been calculated by 5.16-5.18, it is a simple matter to numerically calculate $C_d(\theta)$ & $C_m(\theta)$. Typically 5 to 7 terms in the series were used for each. The advantage of the formulation in Eq.'s (8.2.34) and (8.2.35) is that it shows that $C_d(\theta)$ and $C_m(\theta')$ are well behaved for all θ'.

Derivation for $U_o > U_1$

For this case, R_o is smaller than R_1 so that the velocity input to the sensor is negative through part of the representative waveform. Because of this sign change, the absolute value was not removed from Morison's equation. A Fourier series expansion which incorporates this restriction was not found; therefore, expressions for the instantaneous values of C_d and C_m were not derived. Expressions for $\overline{C_d}$ and $\overline{C_m}$ were found by integrating Equation (8.2.1). This integration was carried out over three intervals defined by angles θ_1 and θ_2 such that:

$$0 < \theta < \theta_1 \quad : \quad U_o + U_1\sin\theta > 0$$

$$\theta_1 < \theta < \theta_2 \quad : \quad U_o + U_1\sin\theta < 0$$

$$\theta < \theta < 2\pi \quad : \quad U_o + U_1\sin\theta > 0$$

where

$$\theta_1 = \pi + \sin^{-1}\left|\frac{U_o}{U_1}\right|$$

$$\theta_2 = 2\pi - \sin^{-1}\left|\frac{U_o}{U_1}\right|$$

To find the expression for $\overline{C_d}$, integrate Equation (8.2.1) over the three regions:

$$\int_o^{2\pi} F^*(\theta)d\theta = \frac{\overline{C_d}}{2}\left[\int_o^{\theta_1} R(\theta)|R(\theta)|d\theta + \int_{\theta_1}^{\theta_2} R(\theta)|R(\theta)|d\theta\right.$$

$$+ \int_{\theta_2}^{2\pi} R(\theta)|R(\theta)|d\theta \Bigg] + \frac{\overline{C_m}\pi^2}{2K^*} \int_{o}^{2\pi} \cos\theta \, d\theta \qquad (8.2.39)$$

where:

$$R(\theta) = R_o + R_1 \sin\theta$$

In the second integral in Equation (8.2.39):

$$R\theta|R\theta| = -(R(\theta))^2$$

Therefore, Equation (8.2.39) can be written:

$$\int_{o}^{2\pi} F^*(\theta)d = \frac{\overline{C_d}}{2}\left[\int_{o}^{2\pi} (R\theta)^2 \, d\theta - 2 \int_{o}^{\theta_2} (R\theta)^2 \, d\theta\right] \qquad (8.2.40)$$

Dividing by π, and substituting for $R(\theta)$:

$$\frac{1}{\pi}\int_{o}^{2\pi} F^*(\theta)d = \frac{\overline{C_d}}{2\pi}\left[\int_{o}^{2\pi} (R_o^2 + 2\,R_oR_1 \sin\theta + R_1^2 \sin^2\theta)d\theta\right.$$

$$\left. - 2\int_{\theta_1}^{\theta_2} (R_o^2 + 2\,R_oR_1 \sin\theta + R_1^2 \sin^2\theta)d\right] \qquad (8.2.41)$$

The left-hand side of Equation (8.2.41) is the definition of A_o given in Equation (8.2.3). Performing the integration on the right-hand side of (8.2.41) yields:

$$A_o = \frac{\overline{C_d}}{2\pi}\left[2\pi R_o^2 + \pi R_1^2 - 2R_1^2(\theta_2 - \theta_1) + 4R_oR_1(\cos\theta_2 - \cos\theta_1)\right.$$

$$\left. - R_1^2(\theta_2 - \theta_1) + \frac{R_1^2}{2}(\sin(2\theta_2) - \sin(2\theta_1))\right] \qquad (8.2.42)$$

Therefore, the expression for $\overline{C_d}$ is:

$$\overline{C_d} = A_o \left[R_o^2 + \frac{R_1^2}{2} \left[1 + \frac{(\theta_1 - \theta_2)}{\pi} \right] + 2 \frac{R_o R_1}{\pi} (\cos \theta_2 - \cos \theta_1) \right.$$

$$\left. + \frac{R_1^2}{4\pi} (\sin 2\theta_2 - \sin 2\theta_1) \right] \qquad (8.2.43)$$

The expression for $\overline{C_m}$ is found by multiplying Equation (8.2.1) by cos θ and integrating over the three regions:

$$\int_o^{2\pi} F^*(\theta) \cos(\theta) d\theta = \frac{\overline{C_d}}{2} \left[\int_o^{2\pi} R^2(\theta) \cos \theta \, d\theta - 2 \int_{\theta_1}^{\theta_2} R^2(\theta) \cos \theta \, d\theta \right]$$

$$+ \frac{C_m \pi^2}{2K^*} \int_o^{2\pi} \cos^2\theta \, d\theta \qquad (8.2.44)$$

Dividing by π, and substituting for R(θ):

$$\frac{1}{\pi} \int_o^{2\pi} F^*(\theta) \cos \theta \, d\theta = \frac{\overline{C_d}}{2} \left[\int_o^{2\pi} (R_o^2 \cos \theta + 2 R_o R_1 \sin \theta \cos \theta \right.$$

$$+ R_1^2 \sin^2\theta \cos \theta) d\theta - 2 \int_{\theta_1}^{\theta_2} (R_o^2 \cos \theta + 2 R_0 R_1 \sin \theta \cos \theta$$

$$\left. + R_1^2 \sin^2\theta \cos \theta) d\theta + \frac{C_m \pi}{2K^*} \int^{2\pi} \cos^2\theta \, d\theta \right] \qquad (8.2.45)$$

The left-hand side of Equation (8.2.45) is the definition of B_1 given in Equation (8.2.3). Performing the integration on the right-hand side of Equation (8.2.45)"

$$B_1 = \frac{\overline{C_d}}{2\pi}\left[\, 2\,R_o^2\,(\sin\theta_2 - \sin\theta_1) - 2\,R_oR_1\,(\sin^2\theta_2 - \sin^2\theta_1)\right.$$

$$\left. - \frac{2}{3}\,R_1^2\,(\sin^3\theta_2 - \sin^3\theta_1)\right] + \frac{C_m\pi^2}{2K^*} \qquad (8.2.46)$$

Rearranging Equation (8.2.46) yields the expression for $\overline{C_m}$:

$$\overline{C_m} = \frac{2K^*}{\pi^2}\left[B_1 + \frac{\overline{C_d}}{\pi}\,(R_o^2\,(\sin\theta_2 - \sin\theta_1) + R_oR_1\,(\sin^2\theta_2\right.$$

$$\left. - \sin^2\theta_1) + \frac{R_1^2}{3}\,(\sin^3\theta_2 - \sin^3\theta_1)\right]$$